NASA Contractor Report 172233

NASA-CR-172233
19840001950

A LIFTING SURFACE THEORY IN ROTATIONAL FLOW

Mawshyong Jack Shiau and C. Edward Lan

THE UNIVERSITY OF KANSAS CENTER FOR RESEARCH, INC.
Flight Research Laboratory
Lawrence, Kansas 66045

Grant NAG1-75
October 1983

National Aeronautics and
Space Administration

Langley Research Center
Hampton, Virginia 23665

Table of Contents

1. List of Symbols

SYMBOL	MEANING
a	$(y_2-y_1)^2$
$\vec{a}$	$(x_1-x)\vec{i} + (y_1-y)\vec{j} + (z_1-z)\vec{k}$ m(ft)
$A', \bar{A}$	$(x_2-x_1)^2 + \beta^2(y_2-y_1)^2$
AR	Aspect ratio
b	Wing span m(ft)
$\vec{b}$	$(x_2-x)\vec{i} + (y_2-y)\vec{j} + (z_2-z)\vec{k}$ m(ft)
b_1	$-2(y-y_1)(y_2-y_1)$
B	$\frac{\partial(\frac{M_\zeta}{M})}{\partial\zeta}$
B'	$[(x_2-x_1)^2(y-y_1)-(x-x_1)(x_2-x_1)(y_2-y_1)]$
$\bar{B}$	$-2[(x-x_1)(x_2-x_1) + \beta^2(y-y_1)(y_2-y_1)]$
BW (I,II)	Summation of Eq. 15 for control point I
C	$\frac{\partial(\frac{M_\eta}{M})}{\partial\eta}$
C_1	$(y-y_1)^2 + z^2$
c_d	Wing sectional profile drag coefficient
C_{D0}	Friction drag coefficient
C_{Di}	Total induced drag coefficient
C_L	Total lift coefficient (Lift/$q_\infty S$)
C_m	Total pitching moment coefficient based on $\bar{c}_0$ (Moment/($q S\bar{c}_0$))
c_r	Wing or tail root chord length m(ft)

C'	$(x_2-x_1)^2+(y-y_1)^2-2(x-x_1)(x_2-x_1)(y-y_1)(y_2-y_1)$ $+(x-x_1)^2(y_2-y_1)^2+\beta^2z^2(y_2-y_1)^2$
$\bar{c}_0$	Mean geometry chord m(ft)
$\bar{C}$	$(x-x_1)^2+\beta^2(y-y_1)^2+\beta^2z^2$
C_p	Pressure coefficient $(P-P_\infty/q_\infty)$
C_{p_ξ}	$\frac{\partial C_p}{\partial \xi}$
D	$(x-\xi)^2+\beta^2(z-\zeta)^2$
D_1	$(x-\xi)^2+\beta^2z^2$
D'_1	$(x-\xi)^2+\beta^2\zeta^2$
DW(I,II)	Summation of Eq. 14 for control point I
$\vec{E}$	$QP'\vec{i}$
f	$\frac{1}{R}\frac{M_\zeta}{M}$
F	Any assumed integration function
G	$(x-\xi)^2+\beta^2(z-\zeta)^2$
G_1	$(\bar{x}_1-\xi)^2+\beta^2(z-\zeta)^2$
$\vec{g}$	$hp'\vec{j}$
h	$\frac{1}{R}\frac{M_\eta}{M}$
$\vec{i},\vec{j},\vec{k}$	Unit vectors along X-, Y-, and Z- axes, respectively
$\vec{l}$	$(x_2-x_1)\vec{i}+(y_2-y_1)\vec{j}+(z_2-z_1)\vec{k}$ m(ft)
M, M_∞	Free stream Mach number
M'	First derivative of Mach number function
M''	Second derivative of Mach number function
$\bar{M}$	Uniform free stream Mach number
M_y	Integration points away from the wing in spanwise direction.
M_a	Integration points in the negative Z direction

M_b	Integration points in the positive Z direction
$\vec{n}$	Unit vector normal to wing surface
N_1	Upstream integration points
N_2	Total integration points on the wing in chordwise direction
N_3	Downstream integration points
N_p	$N_2 = (NW(1)+NW(2))^{N_p}$
N_s	The number of vortex strips in each spanwise section plus one
NW(1)	Number of aerodynamic panels on the wing in chordwise direction
NW(2)	Number of aerodynamic panels on the flap in chordwise direction
P'	Perturbed pressure
P_t	Any point in the flow field
Q	$(x_2-x_1)(y-y_1)-(x-x_1)(y_2-y_1)$
$\bar{Q}$	$(M^2 \bar{M}^2)/R$
q_∞	Free stream dynamic pressure $(\rho_\infty(y,z)V^2(y,z)/2)$ N/m^2 (lb/ft^2)
$\vec{R}$	$X\vec{i} + Y\vec{j} + Z\vec{k}$ m(ft)
R	$[(x-\xi)^2+\beta^2(y-\eta)^2+\beta^2(z-\zeta)^2]^{\frac{1}{2}}$
$\vec{R}_\ell$	$\xi\vec{i} + \eta\vec{j} + \zeta\vec{k}$ m(ft)
R_1, R_β	$[(x-\xi)^2+\beta^2(y-\eta)^2+\beta^2z^2]^{\frac{1}{2}}$
R'_1	$[x_1-\xi)^2+\beta^2(y-\eta)^2+\beta^2z^2]^{\frac{1}{2}}$
S	Arbitrary body surface in a compressible flow $m^2(ft^2)$
S'	A small sphere surface which surrounds a point (ξ,η,ζ) $m^2(ft^2)$

S_w	Wing area $m^2(ft^2)$
V, V_∞	Free stream velocity
$\bar{V}$	The whole flow field volume $m^3(ft^3)$
V'	The volume excluding from $\bar{V}$ the interior of S'
$\bar{v}$	$(y_2-y_1)\,\tau-(y-y_1)$
v_1	$\eta-y$
w	Induced normal downwash velocity $^m/_{sec}$ ($^{ft}/_{sec}$)
$\bar{w}$	Normal downwash angle $\frac{\partial z}{\partial x}c - \alpha$
x,y,z	Wing rectangular coordinates with positive X-axis along axis of symmetry pointing downstream, positive Y-axis pointing to the right, and positive Z-axis pointing upward, m (ft)
$\bar{x}_1$	Integration dummy variable
x_ℓ	Wing leading edge coordinate in the X direction
x_t	Wing trailing edge coordinate in the X direction
X_a	Upstream integration region m (ft)
X_b	Downstream integration region m (ft)
X_{NPG}, X_{NPGH}	Wing and tail neutral point coordinate in chordwise direction
Y_s	Spanwise integration region away from the wing
Y_t	$(y-\eta)^2+(z-\zeta)^2$
Y_t'	$(y-\eta)^2-(z-\zeta)^2$
Y_z	$\beta^2(y-\eta)^2+\beta^2z^2$
Y_z'	$\beta^2(y-\eta)^2-\beta^2z^2$
Z_a	Integration region in the negative Z direction
Z_b	Integration region in the positive Z direction
$z_c(x,y)$	Ordinate of camber surface measured from the X-Y plane m (ft)

Z_d	Vertical distance between wake center and the X-Y plane m (ft)
Z_v	Z coordinate in the flow region

GREEK	MEANING
α, α_w	Wing angle of attack
α_t	Tail angle of attack
β	$(1-\bar{M}^2)^{\frac{1}{2}}$
γ	Vortex density referred to free stream velocity
ΔC_p	Differential pressure coefficient ($C_{p_{lower}} - C_{p_{upper}}$)
θ	Chordwise angular distance (rad)
Λ	Sweep angle of wing leading edge
ρ	Fluid density kg/m^3 ($slug/ft^3$)
ϕ	Spanwise angular distance (rad)
ψ	Vertical angular distance (rad)
$\bar{\psi}$	1/R
ξ, η, ζ	Integration variables in Cartesian system m (ft)
ε	Radius of S'

2. Introduction

When the freestream is nonuniform, the assumption of flow irrotationality becomes inapplicable so that the conventional potential flow theory must be revised (ref. 1). Practical examples of nonuniform freestream include the wing behind a canard wake, a wing or tail situated in the propeller slipstream and airplanes in a wind shear.

The literature on the subject is not extensive. Von Karman and Tsien (ref. 2) developed a lifting line theory for an incompressible nonuniform stream in 1945. Homentcovschi and Barsony (ref. 3) formulated a lifting-surface integral equation for nonuniform incompressible flow with a general stream velocity profile. Hanin and Barsony-Nagy (ref. 4) developed a slender wing theory for a subsonic or low-supersonic nonuniform stream. Later, a lifting line theory (ref. 5) for wings in a subsonic nonuniform stream was presented. Recently, a lifting surface theory for nonuniform supersonic parallel stream (ref. 6) was also developed by them. More recently, experimental investigation of wind shear effect on airfoil aerodynamic characteristics has also been conducted (ref. 7). K. Gersten and D. Gluck (ref. 8) investigated the effect of wing wake on tail characteristics theoretically and experimentally.

In the present investigation, the small-disturbance steady subsonic flow equation for rotational flow is to be solved. The resulting equation is a partial differential equation

with non-constant coefficients. It is transformed into an integral equation through Green's theorem. It is assumed that (1) the Mach number profile M(y,z) or the velocity profile has a nonzero value M(y,o) on the wing plane; (2) there exists a finite second order derivative M"(y,o) on the wing plane, and (3) M'(y,z) is integrable across the stream.

3. Theoretical Development

3.1 Mathematical Formulation

The partial differential equation for small-disturbance subsonic steady rotational flow may be written as (ref. 1)

$$[1-M_\infty{}^2(y,z)]P'_{xx}-2\frac{M_y(y,z)}{M(y,z)}P'_y-2\frac{M_z(y,z)}{M(y,z)}P'_z+P'_{yy}+P'_{zz}=0 \quad (1)$$

where $M(y,z)$ is the undisturbed free stream Mach number and P' is the perturbation pressure. Here, the flow is assumed to be steady, invicid, and compressible past a thin wing at a small angle of attack.

The wing lies in the x-y plane with the positive x axis being streamwise along the wing center line. The origin of the rectangular coordinate system is assumed to be at the wing moment reference point. Let

$$x' = x,\ y' = \beta y,\ z' = \beta z,\ \beta^2 = 1-\bar{M}^2 \quad (2)$$

After the coordinate transformation, equation (1) becomes

$$P'_{x'x'}+P'_{y'y'}+P'_{z'z'} = 2\frac{M_{y'}}{M}P'_{y'}+2\frac{M_{z'}}{M}P'_{z'}+\frac{1}{\beta^2}(M^2-\bar{M}^2)P'_{x'x'} \quad (3)$$

where $\bar{M}$ = constant and is assumed to be a reference uniform Mach number. To use Green's formula:

$$\iiint_V(\bar{\psi}\nabla^2\Omega-\Omega\nabla^2\bar{\psi})\,dv = \iint_S(\bar{\psi}\frac{\partial\Omega}{\partial\eta}-\Omega\frac{\partial\bar{\psi}}{\partial\eta})\,dS \quad (4)$$

let

$$\Omega = p' \quad (5)$$

$$\bar{\psi} = \frac{1}{\bar{R}} = \frac{1}{\sqrt{(x-\xi)^2+\beta^2(y-\eta)^2+\beta^2(z-\zeta)^2}} \quad (6)$$

Consider an arbitrary body with boundary surface S in a compressible flow. Outside the body, the whole flow field has the volume $\bar{V}$. Now, let $P_t(x,y,z)$ be any point in $\bar{V}$.

Then $\bar{\psi}$ is a solution of Laplace's equation:

$$\frac{\partial^2\bar{\psi}}{\partial x'^2} + \frac{\partial^2\bar{\psi}}{\partial y'^2} + \frac{\partial^2\bar{\psi}}{\partial z'^2} = 0 \tag{7}$$

However, the basic solution becomes infinite at P_t so that Green's reciprocal formula can not be applied. To avoid this difficulty, surround P_t with a small sphere S' with radius ε. Let V' be the volume which is obtained by excluding from $\bar{V}$ the interior of S'. V' is bounded by S and S'. Applying Green's reciprocal formula to equation (3), it is obtained that (see Appendix A)

$$\begin{aligned} &P(x',y',z') \\ &= \frac{1}{4\pi}\Big\{ \iint_{S_w}\Big[\frac{1}{R}\frac{\partial P'}{\partial n} - P'\frac{\partial}{\partial n}\Big(\frac{1}{R}\Big)\Big]d\xi d\eta - 2\iint_{S_w} fP'd\xi d\eta \\ &+ 2\iiint_{V'}\frac{\partial f}{\partial \zeta}P'd\xi d\eta d\zeta + 2\iiint_{V'}\frac{\partial h}{\partial \eta}P'd\xi d\eta d\zeta \\ &- \iiint_{V'}\frac{1}{R\beta^2}(M^2-\bar{M}^2)\,P'_{\xi\xi}\,d\xi d\eta d\zeta\Big\} \end{aligned} \tag{8}$$

The boundary condition (the flow tangency condition) is given by (ref. 1)

$$\frac{w(x,y,z)}{V(y,z)} = \frac{\partial z_c}{\partial x} - \alpha \tag{9}$$

Following the linear theory, the boundary condition is satisfied on Z = 0 plane.

From reference 1, the linearized momentum equation in Z component is

$$\rho_\infty(y,z)V_\infty(y,z)\,\frac{\partial w}{\partial x} + \frac{\partial P}{\partial z} = 0 \tag{10}$$

It follows that the downwash in equation (9) can be written as

$$w(x,y,z) = \frac{-1}{\rho_\infty(y,z)V_\infty(y,z)}\int_{-\infty}^{x}\frac{\partial P}{\partial z}(\bar{x}_1,y,z)\,d\bar{x}_1 \tag{11}$$

where the lower limit is chosen in such a way that $w(-\infty,y,z)=0$.

Using equations (8)-(11), after lengthy manipulation, the following final integral equations and boundary conditions for two-dimensional and three-dimensional flows can be obtained (see Appendix A and Appendix B).

(a) Two-Dimensional Flow

The integral equation is given by

$$C_p(x,Z_v) = -\frac{\beta}{2\pi}\int_0^1 \frac{Z_v \Delta Cp}{[(x-\xi)^2+\beta^2 Z_v^2]}d\xi$$

$$- \frac{1}{2\pi\beta}\frac{M_z}{M}(0)\int_0^1 \ell n\left[\frac{\beta^2}{(x-\xi)^2+\beta^2 Z_v^2}\right]\Delta C_p(\xi)\,d\xi$$

$$+ \frac{1}{2\pi\beta}\int\int \left\{\frac{2\beta^2\frac{M_\zeta}{M}(Z_v-\zeta)}{[(x-\xi)^2+\beta^2(Z_v-\zeta)^2]} + \right.$$

$$\left. + B(\zeta)\ \ell n\left[\frac{\beta^2}{(x-\xi)^2+\beta^2(Z_v-\zeta)^2}\right]\right\} C_p(\xi,\zeta)\,d\xi d\zeta$$

$$+ \frac{1}{2\pi\beta^3}\int\int \frac{C_{p_\xi}(\xi,\zeta)(x-\xi)(M^2-\bar{M}^2)}{[(x-\xi)^2+\beta^2(Z_v-\zeta)^2]}d\xi d\zeta \qquad (12)$$

The boundary condition is

$$\bar{w}(x,0) = \frac{\partial z_c}{\partial x} - \alpha$$

$$= \frac{-\beta}{4\pi}\int_0^1 \frac{\Delta Cp(\xi)}{x-\xi}d\xi + \frac{1}{2\pi}\int\int \left[\frac{-\zeta}{|\zeta|}\cdot B(\zeta)\left(\tan^{-1}\frac{x-\xi}{|-\beta\zeta|} + \pi/2\right)\right.$$

$$\left. + \frac{\beta\frac{M_\zeta}{M}(x-\xi)}{(x-\xi)^2+\beta^2\zeta^2}\right] C_p(\xi,\zeta)\,d\xi d\zeta$$

$$+ \frac{1}{4\pi\beta}\int\int \frac{(M^2(\zeta)-\bar{M}^2)\cdot\zeta\cdot C_{p_\xi}(\xi,\zeta)}{[(x-\xi)^2+\beta^2\zeta^2]}d\xi d\zeta \qquad (13)$$

Where $B(\zeta) = \frac{\partial}{\partial\zeta}\left(\frac{M_\zeta}{M}\right)$, M = Mach number, $M_\zeta = \frac{\partial}{\partial\zeta}(M)$, and $Cp_\xi = \frac{\partial}{\partial\xi}C_p(\xi,\zeta)$. C_p is the pressure coefficient.

(b) Three-Dimensional Flow

The integral equation is given by

$$C_p(x,y,Z_v)$$

$$= -\frac{1}{4\pi} \iint_{S_w} \frac{\beta^2 Z_v \cdot \Delta C_p(\xi,\eta)}{[(x-\xi)^2 + \beta^2(y-\eta)^2 + \beta^2 Z_v^2]^{3/2}} \, d\xi d\eta$$

$$- \frac{1}{2\pi} \iint_{S_w} \frac{\frac{M_\zeta}{M}(\eta,0)\,\Delta C_p(\xi,\eta)}{[(x-\xi)^2 + \beta^2(y-\eta)^2 + \beta^2 Z_v^2]^{1/2}} \, d\xi d\eta$$

$$+ \frac{1}{2\pi} \iiint_{V'} \frac{\beta^2 \cdot \frac{M_\zeta}{M}(\eta,\zeta) \cdot (Z_v-\zeta)}{[(x-\xi)^2 + \beta^2(y-\eta)^2 + \beta^2(Z_v-\zeta)^2]^{3/2}} \cdot C_p(\xi,\eta,\zeta)\, d\xi d\eta d\zeta$$

$$+ \frac{1}{2\pi} \iiint_{V'} \frac{B(\eta,\zeta)}{[(x-\xi)^2 + \beta^2(y-\eta)^2 + \beta^2(Z_v-\zeta)^2]^{1/2}} \cdot C_p(\xi,\eta,\zeta)\, d\xi d\eta d\zeta$$

$$+ \frac{1}{2\pi} \iiint_{V'} \frac{\beta^2 \cdot \frac{M_\eta}{M}(\eta,\zeta) \cdot (y-\eta)}{[(x-\xi)^2 + \beta^2(y-\eta)^2 + \beta^2(Z_v-\zeta)^2]^{3/2}} \cdot C_p(\xi,\eta,\zeta)\, d\xi d\eta d\zeta$$

$$+ \frac{1}{2\pi} \iiint_{V'} \frac{C(\eta,\zeta)}{[(x-\xi)^2 + \beta^2(y-\eta)^2 + \beta^2(Z_v-\zeta)^2]^{1/2}} \cdot C_p(\xi,\eta,\zeta)\, d\xi d\eta d\zeta$$

$$+ \frac{1}{4\pi\beta^2} \iiint_{V'} \frac{(x-\xi) \cdot (M^2-\bar{M}^2)}{[(x-\xi)^2 + \beta^2(y-\eta)^2 + \beta^2(Z_v-\zeta)^2]^{3/2}} \cdot C_{p_\xi}(\xi,\eta,\zeta)\, d\xi d\eta d\zeta \qquad (14)$$

The boundary condition is

$$\bar{w}(x,y,z) = \frac{\partial Z_c}{\partial x} - \alpha$$

$$= \frac{\beta^2}{8\pi} \iint_{S_w} \Delta C_p(\xi,\eta) \left\{ \frac{\beta^2(y-\eta)^2 - \beta^2 Z^2}{[\beta^2(y-\eta)^2+\beta^2Z^2]^2} \left(1 + \frac{x-\xi}{[(x-\xi)^2+\beta^2(y-\eta)^2+\beta^2Z^2]^{1/2}}\right) \right.$$

$$\left. - \frac{\beta^2 Z^2 (x-\xi)}{[\beta^2(y-\eta)^2+\beta^2Z^2][(x-\xi)^2+\beta^2(y-\eta)^2+\beta^2Z^2]^{3/2}} \right\} d\xi d\eta$$

$$- \frac{\beta^2}{4\pi} \iint_{S_w} \frac{\frac{M_\zeta}{M}(0) \cdot Z \cdot \Delta C_p(\xi,\eta)}{\beta^2(y-\eta)^2+\beta^2Z^2} \left\{ 1 + \frac{x-\xi}{[(x-\xi)^2+\beta^2(y-\eta)^2+\beta^2Z^2]^{1/2}} \right\} d\xi d\eta$$

$$- \frac{1}{4\pi} \iiint_{V'} C_p(\xi,\eta,\zeta) \cdot \left\{ \frac{\frac{M_\zeta}{M}[(y-\eta)^2-(Z-\zeta)^2] - B(Z-\zeta)[(y-\eta)^2+(Z-\zeta)^2]}{[(y-\eta)^2+(Z-\zeta)^2]^2} \cdot \right.$$

$$\left(1 + \frac{x-\xi}{[(x-\xi)^2+\beta^2(y-\eta)^2+\beta^2(Z-\zeta)^2]^{1/2}} \right)$$

$$\left. - \frac{\beta^2(Z-\zeta)^2 \frac{M_\zeta}{M}(x-\xi)}{[(y-\eta)^2+(Z-\zeta)^2][(x-\xi)^2+\beta^2(y-\eta)^2+\beta^2(Z-\zeta)^2]^{3/2}} \right\} d\xi d\eta d\zeta$$

$$- \frac{1}{4\pi} \iiint_{V'} C_p(\xi,\eta,\zeta) \left\{ \frac{-C(Z-\zeta)[(y-\eta)^2+(Z-\zeta)^2] - 2\frac{M_\eta}{M}(y-\eta)(Z-\zeta)}{[(y-\eta)^2+(Z-\zeta)^2]^2} \cdot \right.$$

$$\left(1 + \frac{x-\xi}{[(x-\xi)^2+\beta^2(y-\eta)^2+\beta^2(Z-^2)^2]^{1/2}} \right)$$

$$\left. - \frac{\beta^2(x-\xi)\frac{M_\eta}{M}(y-\eta)(Z-\zeta)}{[(y-\eta)^2+(Z-\zeta)^2][(x-\xi)^2+\beta^2(y-\eta)^2+\beta^2(Z-\zeta)^2]^{3/2}} \right\} d\xi d\eta d\zeta$$

$$- \frac{1}{8\pi} \iiint_{V'} C_{p_\xi}(\xi,\eta,\zeta) \cdot \frac{(Z-\zeta)(M^2-\bar{M}^2)}{[(x-\xi)^2+\beta^2(y-\eta)^2+\beta^2(Z-\zeta)^2]^{3/2}} d\xi d\eta d\zeta \qquad (15)$$

where

$$B(\eta,\zeta) = \frac{\partial}{\partial}\left(\frac{M_\zeta}{M}\right) \qquad \text{and} \qquad C(\eta,\zeta) = \frac{\partial}{\partial\eta}\left(\frac{M_\eta}{M}\right)$$

3.2 The assumed functional form for C_p

3.2.1 Two-Dimensional Flow

The unknown pressure coefficient C_p is assumed to have a functional form which can be derived by retaining only the first term on the right hand side (R.H.S.) of equation (12). It follows that

$$C_p(\xi,\zeta) = \sum_{j=1}^{K} A_j \frac{-\zeta}{|\zeta|}\left[\tan^{-1}\frac{\xi_{2j}-\xi}{|\beta\zeta|} - \tan^{-1}\frac{\xi_{1j}-\xi}{|\beta\zeta|}\right] \qquad (16)$$

$$C_{p_\xi}(\xi,\zeta) = \sum_{j=1}^{K} A_j \frac{\zeta}{|\zeta|}\left[\frac{|\beta\zeta|}{\beta^2\zeta^2+(\xi_{2j}-\xi)^2} - \frac{|\beta\zeta|}{\beta^2\zeta^2+(\xi_{1j}-\xi)^2}\right] \qquad (17)$$

where ξ_{1j} and ξ_{2j} are chordwise control point locations given by a cosine law distribution as illustrated in Figure 1.

3.2.2 Three-Dimensional Flow

In this case, the assumed functional form for C_p is derived by retaining the first term on the R.H.S. of equation (14) with ξ_1, ξ_2, etc., defined in Figure 2.

$$\begin{aligned} C_p(\xi,\eta,\zeta) = \frac{1}{2\pi}\sum_{j=1}^{N_y}\sum_{i=1}^{N_2} A_{ij}\frac{|\zeta|}{\zeta}\Bigg\{ & \left[\frac{\xi'_{2i}-\xi}{|\xi-\xi'_{2i}|}\left(\tan^{-1}\frac{(\eta-\eta_{2j})|\xi-\xi'_{2i}|}{|\zeta|\sqrt{(\xi-\xi_{2i})^2+\beta^2(\eta-\eta_{2j})^2+\beta^2\zeta^2}}\right)\right. \\ & \left. - \frac{\xi_{2i}-\xi}{|\xi-\xi_{2i}|}\left(\tan^{-1}\frac{(\eta-\eta_{1j})|\xi-\xi_{2i}|}{|\zeta|\sqrt{(\xi-\xi'_{2i})^2+\beta^2(\eta-\eta_{1j})^2+\beta^2\zeta^2}}\right)\right] \\ & - \left[\frac{\xi'_{1i}-\xi}{|\xi-\xi'_{1i}|}\left(\tan^{-1}\frac{(\eta-\eta_{2j})|\xi-\xi'_{1i}|}{|\zeta|\sqrt{(\xi-\xi'_{1i})^2+\beta^2(\eta-\eta_{2j})^2+\beta^2\zeta^2}}\right)\right. \\ & \left. - \frac{\xi_{1i}-\xi}{|\xi-\xi_{1i}|}\left(\tan^{-1}\frac{(\eta-\eta_{1j})|\xi-\xi_{1i}|}{|\zeta|\sqrt{(\xi-\xi_{1i})^2+\beta^2(\eta-\eta_{1j})^2+\beta^2\zeta^2}}\right)\right]\Bigg\} \end{aligned} \qquad (18)$$

$$C_{p_\xi}(\xi,\eta,\zeta)$$

$$= -\frac{1}{2\pi}\sum_{j=1}^{N_2}\sum_{i=1}^{N_1}A_{ij}\frac{1}{\zeta}\left\{\left[\frac{\eta-\eta_{2j}}{1+D_1^2}\left(\frac{1}{\sqrt{(\xi-\xi'_{2i})^2+B_1}}-\frac{(\xi-\xi'_{2i})^2}{[(\xi-\xi'_{2i})^2+B_1]^{3/2}}\right)\right.\right.$$

$$\left.-\frac{\eta-\eta_{1j}}{1+D_2^2}\left(\frac{1}{\sqrt{(\xi-\xi_{2i})^2+B_2}}-\frac{(\xi-\xi_{2i})^2}{[(\xi-\xi_{2i})^2+B_2]^{3/2}}\right)\right]$$

$$-\left[\frac{\eta-\eta_{2j}}{1+D_3^2}\left(\frac{1}{\sqrt{(\xi-\xi'_{1i})^2+B_1}}-\frac{(\xi-\xi'_{1i})^2}{[(\xi-\xi'_{1i})^2+B_2]^{3/2}}\right)\right.$$

$$\left.\left.-\frac{\eta-\eta_{1j}}{1+D_4^2}\left(\frac{1}{\sqrt{(\xi-\xi_{1i})^2+B_2}}-\frac{(\xi-\xi_{1i})^2}{[(\xi-\xi_{1i})^2+B_2]^{3/2}}\right)\right]\right\} \qquad (19)$$

where

$$D_1 = \frac{(\eta-\eta_{2j})\,|\xi-\xi'_{2i}|}{|\zeta|\sqrt{(\xi-\xi'_{2i})^2+\beta^2(\eta-\eta_{2j})^2+\beta^2\zeta^2}}$$

$$D_2 = \frac{(\eta-\eta_{1j})\,|\xi-\xi_{2j}|}{|\zeta|\sqrt{(\xi-\xi_{2i})^2+\beta^2(\eta-\eta_{1j})^2+\beta^2\zeta^2}}$$

$$D_3 = \frac{(\eta-\eta_{2j})\,|\xi-\xi'_{1i}|}{|\zeta|\sqrt{(\xi-\xi'_{1i})^2+\beta^2(\eta-\eta_{2j})^2+\beta^2\zeta^2}}$$

$$D_4 = \frac{(\eta-\eta_{1j})\,|\xi-\xi_{1i}|}{|\zeta|\sqrt{(\xi-\xi_{1i})^2+\beta^2(\eta-\eta_{1j})^2+\beta^2\zeta^2}}$$

$$B_1 = \beta^2(\eta-\eta_{2j})^2+\beta^2\zeta^2$$

$$B_2 = \beta^2(\eta-\eta_{1j})^2+\beta^2\zeta^2$$

4. Numerical Calculation

4.1 Solution procedures

For airfoil problems, equations (12) and (13) are to be solved simultaneously. Similarly, for three-dimensional cases, equations (14) and (15) are to be solved.

To simplify the equations, those double integral terms in equation (15) are reduced to finite sums following the quasi-vortex lattice method (ref. 9). To satisfy the wing boundary condition, the continuous vortex distribution over the wing is replaced by a quasi-continuous one, being continuous chordwise but stepwise constant in the spanwise direction. Thus, the wing surface can be divided into a number of vortex strips with the associated trailing vortices (Figure 3). In any strip, consider a vortex element $\gamma\ dx$ with an arbitrary direction ℓ (Figure 4). The integrals are then reduced to finite sums through the mid-point trapezoidal rule (ref. 9 and Appendix B). Similarly, those double integral terms in equations (14) can be simplified in the same way (see Appendix B).

4.2 Singularities and integration regions

Before proceeding with the numerical integration of integrals, singularities of integrands must be examined.

From the definition of $\bar{\psi}$ in equation (6), it is expected that all integrands will have a singularity at the observation point $x=\xi$, $y=\eta$, $z=\zeta$. To account for this singularity properly, rectangular coordinates are transformed into polar

coordinates by using a cosine law relation (i.e., half circle relation) with separated control and vortex points (ref. 9). Outside the wing, a quarter-circle transformation is used which creates smaller mesh-size near the airfoil or wing. The mesh size is small enough to represent better the rapid change in the pressure coefficient. The detailed integration regions and coordinates transformation are presented in Appendix C.

4.3 Numerical Convergence

The convergence of numerical integration is checked in two ways. One is by comparing integrated results of each term in equations (12), (13), (14), and (15), and the other is by comparing calculated aerodynamic characteristics.

4.3.1 Two-dimensional Flow

The integration schemes for an airfoil are illustrated in Figure 5. Calculated ΔC_p's for different integration schemes are presented in Table 1. It is seen from Table 1 that satisfying equation (12) at 100 points of Z_v through the least square method produces results for ΔC_p which can be obtained by satisfying equation (12) only at $Z_v = 0.05$ (Case No. 8 in Table 1). Note that the airfoil chord length is taken to be unity. Therefore, to save computing time, equation (12) will be satisfied only at $Z_v = 0.05$ from now on. For a wing, this is revised to be $Z_v = 0.05\ \bar{C}_o$, where $\bar{C}_o$ is the mean geometric chord.

It should be noted that the so-called least square method for satisfying equation (12) is based on the following concept.

By choosing N points of (x, Z_v) in the x - z plane, equation (12) can be integrated to result in N values of differences between both sides of equation (12). Let these values be denoted by F_k. Let

$$F_k = \sum_i b_{ik} \cdot \Delta C_{p_i} + \sum_i C_{i_k} A_i \qquad (20)$$

where K = 1,2....N.

If the sum of F_k^2 is differentiated with respect to A_j, and the results are set to zero, it is obtained that

$$\sum_{K=1}^{N} \frac{\partial F_K^2}{\partial A_j} = 0, \quad j = 1, J \qquad (21)$$

This results in a set of simultaneous homogeneous equations for C_p's and A's:

$$\sum_k C_{jk} b_{ik} \quad \Delta C_{p_i} + \sum_k C_{jk} C_{ik} \quad A_i = 0 \qquad (22)$$

4.3.2 Three-dimensional flow

The spanwise integration regions are illustrated in Figure 6. Using an elliptic wing of AR = 10.91, convergence of numerical integration of integrals in equation (15) has also been investigated. Note that all integrations are performed through the midpoint trapezoidal rule after the coordinate transformation described in Section 4.2. From this study, it is determined that the following values for integration parameters are appropriate: $N_1 = 6$, $N_p = 0$, $N_3 = 5$, $M_y = 5$, $M_1 = 2$, $X_a = 2.5 \times C_r$, $X_b = 0.8 \times C_r$, $Y_s = 0.5 \times b/2$, and $Z_a = Z_b = 3.0 \times b/2$.

4.4 Freestream profiles

In the present investigation, the freestream velocity profiles are of three types only--jet, wake, and linear shear profiles. These are illustrated in Figures 7 and 8. The jet or wake stream profiles are described by

$$M(Z) = M_1 + (M_0 - M_1) \exp\left(-(z-z_d)^2/H^2\right) \qquad (23)$$

On the other hand, the linear shear profile is given by

$$\begin{aligned} M &= M_1 && \text{for } z \geq H \\ &= 1/2\ (M_1+M_2) + 1/2\ (M_1-M_2)\ (z-z_d)/H && \text{for } -H \leq z \leq H \\ &= M_2 && \text{for } z \leq H \end{aligned} \qquad (24)$$

5. Numerical Results and Discussions

In this section, some numerical results by the present method will be presented. Comparison with theoretical results from references 5 and 10 will be made first.

5.1 Two-dimensional Joukowski Airfoil in a Jet Stream

Results of the present thin airfoil theory for a 2-D Joukowski airfoil as shown in Table 1 are compared with those obtained by a finite difference method (reference 10) in Figure 9. It is seen that the present predicted pressure peak is more aft and the peak magnitude is slightly less than those given by reference 11. Thickness effect may be responsible for the discrepancy between these two methods.

5.2 Elliptic Wing in the Jet and Wake

Elliptic wings of various aspect ratios have been extensively investigated in reference 5 by the lifting-line approach. The present results for a wing of AR $=10.0/\sqrt{1.-M_o^2}$ compared with those from reference 5 in Figure 10, in jet and wake flow. It is seen from Figure 10 that the agreement between two theories is good except when M_o is large in the wake flow. From the general linearized partial differential equation for the rotational flow (eqs. 3 and 23), it is known that not only $(1-M_o)^{1/2}$ AR and M_o/M_1 are important similarity parameters, but also is M_o. The theory of reference 5 does not show the dependence of results on M_o independently. The ordinate in Figure 10 is C_L/C_{L_o}, where C_L is the lift coefficient in nonuniform flow based on the local velocity

V(o) and density $\rho(o)$. C_{L_o} is the lift coefficient of the same wing at the same angle of attack α in uniform stream.

The results also show that the effect of a nonuniform stream on the lift and induced drag becomes stronger with increasing ratio of maximum to minimum Mach numbers of the stream.

5.3 Effect of Wing Wake on Tail Characteristics

As shown in Fig. 11, a tail surface is frequently situated in a non-uniform flow field caused by the wake of a wing. The experimental results for a wing-tail configuration shown in Fig. 12 were obtained by W. Siegler (ref.13). In the present calculation, the wing-section drag coefficient is needed. Its assumed values are shown in Fig. 13 by extrapolating available data for NACA 0012 airfoil which was used in the experiment. The relation between wing and tail angles of attack is shown in Fig. 14 and the wake location in Fig. 15. (See Appendix D for a detailed calculation of the wing wake). The results by the present method for this configuration are shown in Fig. 16 together with experimental data.

In Fig. 16(a), it is seen that with the wing at low angles of attack, the wing wake is far below the tail and has no effect on the tail. With increasing angles of attack, the lift of tail increases until a certain angle of attack (24^{o}) is reached. Then the tail enters the wake center of the wing and the tail lift decreases as the angle of attack is increased further.

Fig. 16(b) shows that the predicted pitching moment exhibits the same trend as the experimental data from reference 13.

However, the predicted magnitude is too negative, even in the uniform flow. At a certain angle of attack, the tail enters the wing wake, and the nose-down contribution of the tail to the total moment is reduced, resulting in unstable pitching moment characteristics.

5.4 Rectangular Wing of AR = 3.3 in the Wake

Theoretical longitudinal aerodynamic characteristics of a rectangular wing of AR = 3.3 in the wake stream are shown in Figure 17. In Figure 17(a), it shows that as the wake center is far away below the wing, the effect of reduced dynamic pressure is small. Due to the positive velocity gradient, the vorticity is in the same sense as the circulation around the wing. As a result, there is a gain of lift. When the wake center moves closer to the wing, the effect of reduced dynamic pressure becomes more important and the lift is reduced. After the wake center moves up and away from the wing plane, the negative velocity gradient contributes a loss in lift compared to the lift gain when the wake center is at the same distance below the wing. As the wake center moves further away, the lift will get close to results of the uniform flow.

In Figure 17(b), it is seen that as the wake center stays below the wing, the positive velocity gradient makes a significant contribution to the leading edge thrust. At Z_d=-0.7071, the induced drag is calculated to be negative due to large positive velocity gradient. Whether this is possible in reality requires further study. On the contrary, the leading edge thrust is reduced when the wake center is above the wing.

In Figure 17(c), the aerodynamic center is shown to shift forward (i.e., more negative $\partial C_m/\partial C_L$) when the wake center is

below the wing and moves backward when the wake center is above the wing. Again, the velocity gradient effect is responsible for this difference.

Figure 17(d) indicates that the pitching moment becomes less negative as the wing moves into the wake. This trend is consistent with the results presented in reference 8. Within a certain range of angles of attack, as the wake moves toward the wing, $\partial C_m/\partial\alpha$ becomes positive, contributing to pitch instability of the airplane.

5.5 Rectangular Wing (AR = 7.2) in the Linear Sheared Flow

Theoretical longitudinal aerodynamic characteristics of a rectangular wing of AR = 7.2 in the linear sheared flow are shown in Figure 18.

In Figure 18(a), it is seen that the lift is decreased due to the local dynamic pressure effect. However, the positive velocity gradient makes a positive contribution to lift as mentioned earlier. With $Z_d = 0.0$ and $M_o = 0.15$, the lift is slightly greater than those in uniform flow ($M_\infty = 0.15$) due to this positive velocity gradient effect. For the sheared flow, since the second derivative of the Mach number profile, $M''(\zeta)$, is zero, the change of lift and induced drag coefficients is much lower than those in the wake or jet.

In Figure 18(b), since the velocity gradient effect is almost the same for each case, the difference in lift-drag ratio is mostly due to the local dynamic pressure effect.

As shown in Figure 18(c), the aerodynamic center is not much changed in the linear sheared flow from that in the uniform flow. This is because nonuniform flow effect makes the same contribution to both the lift and pitching moment.

5.6 Plane Delta Wing (AR = 1.4559, Λ= 70°) in the Jet

It is assumed that the suction analogy of Polhamus (ref. 12) is still applicable in a nonuniform flow. The vortex lift calculation through the method of suction analogy described in reference 11 is applied to a wing in the nonuniform free stream. The longitudinal aerodynamic characteristics of a plane delta wing of 70-degree sweep by the attached flow theory and by the vortex lift theory are shown in Figure 19. It is seen from Figure 19(a) the vortex lift increase is slightly larger in the jet stream than that in the uniform stream. Figure 19(b) shows that the lift-drag ratio is increased in the jet either in the attached flow or in the vortex flow as compared with that in the uniform flow. This is because the wing is at the jet center, so that the local dynamic pressure effect plays the main role. In Figure 19(c), it is seen that $\frac{\partial C_m}{\partial C_L}$ is not much affected by the nonuniform flow effect at low lift coefficients. At high lift coefficients, $|\frac{\partial Cm}{\partial C_L}|$ is slightly reduced by the jet flow.

6. Conclusions

A lifting-surface theory for the subsonic compressible nonuniform flow has been developed. The theory not only accounts for different local dynamic pressures, but also the effect of velocity gradient. Comparison with limited known results show that the present theory is reasonably accurate. Numerical results indicate that there is a gain in lift if the wing is in a region with a positive velocity gradient.

Based on the assumption that the suction analogy is still applicable in a nonuniform flow, results for a 70°-delta wing show that the vortex lift is enhanced by a jet flow.

The present theory can be applied to any type of free stream profiles with variations in both spanwise and vertical directions.

REFERENCES

1. Sears, W.R., "Small Perturbation Theory," in General Theory of High Speed Aerodynamics, edited by W.R. Sears, Princeton University Press.

2. Von Karman, T. and Tsien, H.S., "Lifting-Line Theory for a Wing in Nonuniform Flow," Quarterly of Applied Mathematics, Vol. 3, April 1945, p. 1-11.

3. Homentcovschi, D. and Barsony-Nagy, A., "A Linearized Theory of Three-Dimensional Airfoils in Nonuniform Flow," Acta Mechanica. Vol. 24,1976. PP. 63-86.

4. Hanin, M. and Barsony-Nagy, A., "Slender Wing Theory for Nonuniform Stream," AIAA Journal, Vol. 18, April 1980, p. 381-384.

5. Barsony-Nagy, A. and Hanin, M., "Aerodynamics of Wings in Subsonic Shear Flow," AIAA Journal, Vol. 20, April 1982, p. 451-456.

6. Barsony-Nagy, A. and Hanin, M., "Aerodynamics of Wings in Supersonic Shear Flow," AIAA-82-0939. AIAA/ASME 3rd Joint Thermophysics, Fluids, Plasma, and Heat Transfer Conference, June 7-11, 1982, St. Louis, Missouri.

7. Payne, F.M., "An Experimental Investigation of the Influence of Vertical Wind Shear on the Aerodynamic Characteristics of An Airfoil," AIAA-82-0214. AIAA 20th Aerospace Science Meeting.

8. Gersten, K, and Glück, "On the Effect of Wing Wake on Tail Characteristics," AGARD-CP-262, Aerodynamics Characteristics of Controls, 1970, p. 261-268.

9. Lan, C.E., "A Quasi-Vortex-Lattice Method in Thin Wing Theory," Journal of Aircraft, Vol. 11, No. 9, Sept. 1974, p. 518-527.

10. Chow, F., Krause, E., Liu, C.H. and Mao, J., "Numerical Investigation of an Airfoil in a Nonuniform Stream," Journal of Aircraft, Vol. 7, No. 6, Nov.-Dec. 1970.

11. Lan, C.E. and Chang, J.F., "Calculation of Vortex Lift Effect for Cambered Wing by Suction Analogy," NASA CR-3449, 1981.

12. Polhamus, E.C., "A Concept of the Vortex Lift of Sharp Edge Delta Wing Based on a Leading-Edge-Suction Analogy," NASA TN D-3767, Dec. 1966.

13. Siegler, W. and Wagner, B., "Experimentelle Untersuchungen zum Uberziehverhalten von Flugzeugen mit T-Leitwerk," ZFW Heft 3, 1978, pp. 156-165.

14. Silverstein, A., Katzoff, S. and Bullivant, W.K., "Downwash and Wake Behind Plain and Flapped Airfoils," NACA TR651, 1939.

15. Silcerstein, A. and Katzoff, S., "Design Charts for Predicting Downwash Angles and Wake Characteristics Behind Plain and Flapped Wings," NACA TR.648, 1939.

16. Schlichting, H. and Truckenbrodt, E., Aerodynamics of the Airplane, McGraw-Hill, Inc., 1979.

APPENDIX A

Integral equations for the 2-D Small-Disturbance Subsonic Nonuniform Flow

The detailed derivation for equations (12) and (13) is given below.

A.1 A General Integral Equation

Applying Green's reciprocal formula to equation (3), it is obtained that

$$\iiint_{V'} \frac{1}{R}\left[2\frac{M_\eta}{M}P'_\eta + 2\frac{M_\zeta}{M}P'_\zeta + \frac{1}{\beta^2}(M^2-\bar{M}^2)P'_{\xi\xi}\right]d\xi\,d\eta\,d\zeta$$
$$= \iint_S \left[\frac{1}{R}\frac{\partial P'}{\partial n} - P'\frac{\partial}{\partial n}\left(\frac{1}{R}\right)\right]dS + \iint_{S'}\left[\frac{1}{R}\frac{\partial P'}{\partial n} - P'\frac{\partial}{\partial n}\left(\frac{1}{R}\right)\right]dS' \qquad (A.1)$$

Now, on S' (a small spherical surface),

$$\frac{\partial}{\partial n}\left(\frac{1}{R}\right)\Big]_{R=\varepsilon} = -\left(\frac{\partial}{\partial R}\left(\frac{1}{R}\right)\right)_{R=\varepsilon} = \frac{1}{\varepsilon^2}$$

The direction of normal differential of S' points away from V', i.e., towards the interior of sphere. It follows that the second integral on the right-hand-side of equation (A.1) becomes

$$\iint_{S'}\left(\frac{1}{\varepsilon}\frac{\partial P'}{\partial n} - P'\frac{1}{\varepsilon^2}\right)dS = \frac{1}{\varepsilon}\iint_S \frac{\partial P'}{\partial n}dS - \frac{1}{\varepsilon^2}\iint_{S'} P'dS$$

as $\varepsilon \to 0$, $\varepsilon^2 \to 0$, and $S' \to 0$. Hence, the first term in equation (A.1), $\frac{1}{\varepsilon}\iint \frac{\partial P'}{\partial n}dS \longrightarrow 0$.

Note that $\frac{1}{4\pi\varepsilon^2}\iint_{S'} P'dS$ is the arithematic mean value of p' on S' and tends to p'(x,y,z) as $\varepsilon \to 0$. Therefore,

$$\frac{1}{\varepsilon^2}\iint_{S'} P'dS = 4\pi P'$$

Equation A.1 now becomes

$$\iiint_{V} \frac{1}{R}\left[2\frac{M_\eta}{M}P'_\eta + 2\frac{M_\zeta}{M}P'_\zeta + \frac{1}{\beta^2}(M^2-\bar{M}^2)P'_{\xi\xi}\right]d\xi\,d\eta\,d\zeta$$
$$= \iint_S \left[\frac{1}{R}\frac{\partial P'}{\partial n} - P'\frac{\partial}{\partial n}\left(\frac{1}{R}\right)\right]d\xi\,d\eta - 4\pi P' \qquad (A.2)$$

where $R = \sqrt{(x-\xi)^2+\beta^2(y-\eta)^2+\beta^2(z-\zeta)^2}$

Let $\frac{1}{R}\frac{M_\zeta}{M} = f(\xi,\eta,\zeta)$

$$f P'_\zeta = \frac{\partial}{\partial\zeta}(fP') - \frac{\partial f}{\partial\zeta}P'$$

Therefore,

$$\iiint_{V'} f P'_\zeta \, d\xi\, d\eta\, d\zeta = \iiint \left(\nabla\cdot\vec{g} - \frac{\partial f}{\partial\zeta}P'\right) d\xi\, d\eta\, d\zeta$$

where $g = \vec{k}fp'$.

From the divergence theorem, the above equation can be written as

$$\iiint_{V'} f P'_\zeta \, d\xi\, d\eta\, d\zeta = \iint_{S+S'} f P' \vec{k}\cdot\vec{n}\, dS - \iiint_{V'} \frac{\partial f}{\partial\zeta} P' \, d\xi\, d\eta\, d\zeta \qquad (A.3)$$

Similarly, let

$$\frac{1}{R}\frac{M_\eta}{M} = h(\xi,\eta,\zeta).$$

$$\iiint_{V'} h P'_\eta \, d\xi\, d\eta\, d\zeta$$

$$= \iiint \left(\nabla\cdot\vec{g} - \frac{\partial h}{\partial\eta}P'\right) d\xi\, d\zeta = \iint_{S+S'} h P' d\xi\, d\zeta - \iiint_{V'} \frac{\partial h}{\partial\eta} P' d\xi\, d\eta\, d\zeta \qquad (A.4)$$

where $\vec{g} = \vec{j}hp'$.

Substituting equations (A.3) and (A.4) into equation (A.1), equation (A.1) becomes

$$P(x,y,z) = \frac{1}{4\pi}\left\{ \iint_{S_W} \left[\frac{1}{R}\frac{\partial P'}{\partial n} - P'\frac{\partial}{\partial n}\left(\frac{1}{R}\right)\right] dS - 2\iint_{S_W} f P' dS + 2\iiint_{V'} \frac{\partial f}{\partial\zeta} P' \, dv \right.$$

$$\left. + 2\iiint_{V'} \frac{\partial h}{\partial\eta} P' dv - \iiint_{V'} \frac{1}{R\beta^2}\left(M^2 - \bar{M}^2\right) P'_{\xi\xi}\, dv \right\} \qquad (A.5)$$

Equation (A.5) is the general integral equation for the small-disturbance subsonic nonuniform flow.

Now, apply the boundary condition equation (equation 11) to each term (except the first term) on the right hand side of equation (A.5) and perform the integration from $\eta=-\infty$ to $\eta = \infty$ for the two-dimensional case. Let

$$R=\sqrt{(x-\xi)^2+\beta^2(y-\eta)^2+\beta^2(z-\zeta)^2} \quad , \quad R_1=\sqrt{(x-\xi)^2+\beta^2(y-\eta)^2+\beta^2 z^2}$$

$$D=(x-\xi)^2+\beta^2(z-\zeta)^2 \quad , \quad D_1=(x-\xi)^2+\beta^2 z^2$$

$$D_1'=(x-\xi)^2+\beta^2\zeta^2 \quad , \quad G=(x-\xi)^2+\beta^2(z-\zeta)^2$$

$$G_1=(\bar{x}_1-\xi)^2+\beta^2(z-\zeta)^2$$

Several terms in equation (A.5) will be simplified separately in the following:

A.2 $$P_1=-\frac{1}{4\pi}\iint_{S_W}^{\infty}_{-\infty} P'\frac{\partial}{\partial n}\left(\frac{1}{R_1}\right)d\eta\,d\xi \qquad (A.6)$$

Remember, η is positive outward away from the flow field, so that $\eta = -Z$ for the upper surface. It follows that

$$\frac{\partial}{\partial}\left(\frac{1}{R_1}\right)=-\frac{\partial}{\partial z}\left(\frac{1}{R_1}\right)=\frac{\beta^2 z}{R_1^3} \qquad (A.7)$$

Substituting equation (A.7) into equation (A.6), it is obtained that

$$P_1=-\frac{\beta}{2\pi}\int\frac{z\Delta P'}{D_1}\,d\xi \qquad (A.8)$$

The boundary condition requires that the flow be tangent to the camber surface in the thin airfoil theory. This condition can be written as

$$\frac{w(x,0)}{V_0(0)}=\frac{\partial z_c}{\partial x}-\alpha \qquad (A.9)$$

where z_c is the camber. To find the downwash w(x,z), equation (10)

is integrated to give

$$w_1(x, z) = -\frac{1}{\rho(z)V(z)}\int_{-\infty}^{x}\frac{\partial p_1}{\partial z}\,d\bar{x}_1 \qquad (A.10)$$

where the lower limit is chosen in such a way that $w(-\infty, Z)=0$. Substituting equation (A.8) into equation (A.10), the following equation can be obtained

$$\frac{w_1(x,0)}{V_\infty(0)} = \frac{\partial z_c}{\partial x} - \alpha = -\frac{\beta}{4\pi}\int_0^1 \frac{\Delta C_p(\xi)}{x-\xi}\,d\xi \qquad (A.11)$$

where

$$\Delta C_p = \frac{\Delta p'}{\frac{1}{2}\rho(0)V^2(0)}$$

A.3

$$p_2 = -\frac{1}{2\pi}\frac{M_\infty(0)}{M}\iint_{S_w}\frac{\Delta p'}{R_1}\,d\xi\,d\eta \qquad (A.12)$$

Let $\eta - y = v_1$

$$\int_{-\infty}^{\infty}\frac{d\eta}{R_1} - \frac{1}{\beta}\ln 4l^2$$

$$= 2\int_0^{\infty}\frac{dv_1}{\beta\sqrt{v_1^2+\frac{D_1}{\beta^2}}} - \frac{1}{\beta}\ln 4l^2$$

$$= \lim_{l\to\infty}\frac{2}{\beta}\int_0^{l}\frac{dv_1}{\sqrt{v_1^2+\frac{D_1}{\beta^2}}} - \frac{1}{\beta}\ln 4l^2$$

$$= \lim_{l\to\infty}\frac{2}{\beta}\ln\left|v_1+\sqrt{v_1^2+D_1/\beta^2}\right| - \frac{1}{\beta}\ln 4l^2$$

$$= \frac{1}{\beta}\ln\frac{\beta^2}{D_1} \qquad (A.13)$$

Substituting equation (A.13) into equation (A.12), it is obtained that

$$p_2 = -\frac{1}{2\pi\beta}\frac{M_\infty(0)}{M}\int\ln\left(\frac{\beta^2}{D_1}\right)\Delta p'(\xi)\,d\xi \qquad (A.14)$$

Similarly, applying the boundary condition equations Eq.(9) and equation (11) to equation (A.14), it can be shown that

$$w_2(x,0) = 0,$$

since $\frac{\partial P_2}{\partial z}(x,0) = 0.$

A.4 $$P_3 = \frac{1}{2\pi}\iiint \frac{\partial f}{\partial \zeta} p' d\xi d\eta d\zeta \qquad (A.15)$$

Integrating from $\eta=-\infty$ to $\eta=\infty$ for equation (A.15), it is obtained that

$$P_3 = \frac{1}{2\pi}\iiint_{-\infty}^{\infty} \frac{M_\zeta \beta^2 (z-\zeta) P'(\xi,\zeta)}{M R^3} d\eta d\xi d\zeta + \frac{1}{2\pi}\iiint_{-\infty}^{\infty} \frac{B(\zeta) P'(\xi,\zeta)}{R} d\eta d\xi d\zeta$$

$$= \frac{1}{2\pi\beta}\iint \frac{2\beta^2 \frac{M_\zeta}{M}(z-\zeta) P'}{D} d\xi d\zeta + \frac{1}{2\pi\beta}\iint B(\zeta) \ln \frac{\beta^2}{D} d\xi d\zeta \qquad (A.16)$$

After applying equation (9) and equation (11) to equation (A.16), the following integrals are needed:

$$\int_{-\infty}^{\infty} \frac{d\eta}{R^5} = \frac{4}{3\beta D^2} \qquad (A.17)$$

$$\int_{-\infty}^{x} \frac{d\bar{x}_1}{G_1} = \frac{1}{\beta|z-\zeta|}\left(\tan^{-1}\frac{x-\xi}{\beta|z-\zeta|} + \pi/2\right) \qquad (A.18)$$

It follows that

$$\frac{W(x,y,0)}{V(y,0)} = \frac{\partial z_c}{\partial x} - \alpha$$

$$= \frac{1}{2\pi}\iint \frac{-\zeta}{|-\zeta|} \cdot B(\zeta)\left(\tan^{-1}\frac{x-\xi}{\beta|-\zeta|} + \pi/2\right) C_p(\xi,\zeta) d\xi d\zeta$$

$$+ \frac{1}{2\pi}\iint \frac{\beta \frac{M_\zeta}{M}(x-\xi) C_p(\xi,\zeta)}{D_1'} d\xi d\zeta \qquad (A.19)$$

where

$$C_p(\xi,\zeta) \equiv \frac{P'}{\frac{1}{2}\rho(y,0) V_\infty^2(y,0)} \qquad (A.20)$$

A.5 $$P_6 = -\frac{1}{4\pi\beta^2}\iiint \frac{M^2-\bar{M}^2}{R} P'_{\xi\xi}\, d\xi d\eta d\zeta \qquad (A.21)$$

Let $$\bar{Q}(\xi,\eta,\zeta) = \frac{M^2-\bar{M}^2}{R}$$

$$\bar{Q}P'_{\xi\xi} = \frac{\partial}{\partial\xi}(\bar{Q}P'_{\xi}) - \frac{\partial\bar{Q}}{\partial\xi}P'_{\xi}$$

$$\vec{E} = \bar{Q}P'_{\xi}\,i$$

Applying the divergence theorem to equation (A.21), it is obtained that

$$\iiint_{V'} \bar{Q}P'_{\xi\xi}\,dV = \iiint_{V'} (\nabla\cdot\vec{E} - \frac{\partial\bar{Q}}{\partial\xi}P'_{\xi})\,dV$$

$$= \iint_{S} \bar{Q}P'_{\xi}\,\vec{i}\cdot\vec{n}\,dS - \iiint_{V'}\frac{\partial\bar{Q}}{\partial\xi}dV$$

$$= \iint_{S} \bar{Q}P'_{\xi}\,d\eta d\zeta - \iiint_{V'}\frac{\partial\bar{Q}}{\partial\xi}dV \qquad (A.22)$$

($\bar{Q}P'_{\xi}$ on S is 0)

It follows that

$$P_6 = \frac{1}{2\pi\beta^2}\iint \frac{P'_{\xi}(x-\xi)(M^2-\bar{M}^2)}{\beta D}\,d\xi d\zeta \qquad (A.23)$$

From the boundary conditions (eq. (9) and eq. (11)), it is finally obtained that

$$\frac{W_6(x,0)}{V(y,0)} = \frac{\partial z_c}{\partial x} - \alpha = \frac{-1}{4\pi\beta^2}\iint \frac{\zeta(M^2(\zeta)-\bar{M}^2)}{D'_1}C_{P_\xi}\,d\xi d\zeta \qquad (A.24)$$

Note:

$$\int_{-\infty}^{\infty} \frac{d\eta}{R_1^3} = \frac{2}{\beta D_1} \tag{A.25}$$

$$\int_{-\infty}^{\chi} \frac{\tilde{X}_1 \, d\tilde{X}_1}{G_1^2} = \frac{\xi\chi - [\xi^2 + \beta^2(z-\zeta)^2]}{2\beta^2(z-\zeta)^2 \cdot D} + \frac{\xi}{2\beta^2(z-\zeta)^2} \int_{-\infty}^{\chi} \frac{dx_1}{G_1} \tag{A.26}$$

$$\int_{-\infty}^{\chi} \frac{d\tilde{X}_1}{G_1^2} = \frac{1}{2\beta^2(z-\zeta)^2} \left[\frac{\chi - \xi}{q} + \frac{1}{\beta|z-\zeta|} \left(\tanh^{-1} \frac{\chi - \xi}{\beta|z-\zeta|} + \pi/2 \right) \right] \tag{A.27}$$

$$\int_{-\infty}^{\chi} \frac{(\tilde{x}_1 - \xi)}{G_1^2} d\tilde{x}_1 = \frac{-1}{2q} \tag{A.28}$$

APPENDIX B

Integral Equations for the 3-D Small-Disturbance Subsonic Nonuniform Flow

To derive the wing boundary condition (eq. 15), equation (A.15) will be used again. Several terms in equation (A.5) are simplified below.

For simplicity, the following symbols are introduced:

$$R=\sqrt{(x-\xi)^2+\beta^2(y-\eta)^2+\beta^2(z-\zeta)^2} \quad , R_1=\sqrt{(x-\xi)^2+\beta^2(y-\eta)^2+\beta^2 z^2}$$

$$R_1'=\sqrt{(x_1-\xi)^2+\beta^2(y-\eta)^2+\beta^2 z^2} \quad , D=(x-\xi)^2+\beta^2(z-\zeta)^2$$

$$D_1=(x-\xi)^2+\beta^2 z^2 \quad , D_1'=(x-\xi)^2+\beta^2\zeta^2$$

$$Y_z=\beta^2(y-\eta)^2+\beta^2 z^2 \quad , Y_z'=\beta^2(y-\eta)^2-\beta^2 z^2$$

$$G=(x-\xi)^2+\beta^2(z-\zeta)^2 \quad , G_1=(\bar{x}_1-\xi)^2+\beta^2(z-\zeta)^2$$

$$Y_t=(y-\eta)^2+(z-\zeta)^2 \quad , Y_t'=(y-\eta)^2-(z-\zeta)^2$$

B.1
$$P_1=-\frac{1}{4\pi}\iint P'\frac{\partial}{\partial n}\left(\frac{1}{R_1}\right)d\xi\,d\eta \qquad (B.1)$$

After applying (eq.9) and (eq. 11), the following equations can be obtained:

$$W_1(x,y,z)=\frac{-1}{\rho_\infty(y,z)\,V_\infty(y,z)}\int_{-\infty}^{x}\frac{\partial P_1}{\partial z}(\bar{x}_1,y,z)\,d\bar{x}_1 \qquad (B.2)$$

$$\int_{-\infty}^{x}\frac{d\bar{x}_1}{R_1^3}=\frac{1}{Y_z}\left(1+\frac{x-\xi}{R_1}\right) \qquad (B.3)$$

$$\int_{-\infty}^{x}\frac{d\bar{x}_1}{R_1'^5}=\frac{x-\xi}{3Y_z'R_1}\left(\frac{1}{R_1^2}+\frac{2}{Y_z}\right)+\frac{2}{3}\frac{1}{Y_z^2} \qquad (B.4)$$

It follows that

$$\frac{W_1(x,y,z)}{V_\infty(y,z)} = \frac{\beta^2}{8\pi}\iint \Delta C_p \left[\frac{\gamma_z'}{\gamma_z}\left(1+\frac{x-\xi}{R_1}\right) - \frac{\beta^2 z^2 (x-\xi)}{\gamma_z R_1^3}\right] d\xi\, d\eta \qquad (B.5)$$

B.2

$$P_2 = -\frac{1}{2\pi}\iint_S f\, P'\, dS \qquad (B.6)$$

where

$$f = \frac{1}{R}\,\frac{M_\xi}{M}$$

Applying equation (11) to equation (B.6), it is obtained that

$$W_2 = \frac{1}{\rho_\infty V_\infty}\int_{-\infty}^{x} \frac{\partial P_2}{\partial z}(\bar{x}_1, y, z)\, d\bar{x}_1 \qquad (B.7)$$

It follows that

$$\frac{W_2(x,y,z)}{V_\infty(y,z)} = -\frac{1}{4\pi}\iint \frac{\frac{M_\xi}{M}(0)\, z\cdot \Delta C_p}{(y-\eta)^2+z^2}\left\{1+\frac{x-\xi}{R_1}\right\} d\xi\, d\eta \qquad (B.8)$$

B.3

$$P_3 = \frac{1}{2\pi}\iiint \frac{\partial f}{\partial \zeta} P'\, d\xi\, d\eta\, d\zeta \qquad (B.9)$$

where

$$\frac{\partial f}{\partial \zeta} = \frac{\frac{M_\xi}{M}\beta^2(z-\zeta)}{R^3} + \frac{B(\eta,\zeta)}{R}$$

Applying equation (11) to equation (B.9), the following integral is obtained:

$$W_3 = -\frac{1}{\rho_\infty V_\infty}\int_{-\infty}^{x} \frac{\partial P_3}{\partial z}\, dx_1 \qquad (B.10)$$

where

$$\frac{\partial P_3}{\partial z} = \frac{1}{2\pi}\iiint \left\{ \frac{\beta^2\left[\frac{M_\xi}{M} - B(z-\zeta)\right]P'}{R^3} - \frac{3\beta^4(z-\zeta)^2\frac{M_\xi}{M}P'}{R^5}\right\} d\xi\, d\eta\, d\zeta \qquad (B.11)$$

It follows that

$$\frac{W_3(x,y,z)}{V_\infty(y,z)} = -\frac{1}{4\pi}\iiint C_p(\xi,\eta,z)\cdot\left\{\frac{\frac{M_\zeta}{M}Y_t' - B(z-\zeta)Y_t}{Y_t^2}\left(1+\frac{x-\xi}{R}\right)\right.$$

$$\left. - \frac{\beta^2(z-\zeta)^2\frac{M_\zeta}{M}(x-\xi)}{Y_t\cdot R^3}\right\} d\xi\, d\eta\, d\zeta \qquad (B.12)$$

B.4 $$P_5 = \frac{1}{2\pi}\iiint \frac{\partial h}{\partial \eta} P' d\xi d\eta d\zeta \qquad (B.13)$$

where

$$\frac{\partial h}{\partial \eta} = \frac{\frac{M_\eta}{M}\beta^2(y-\eta)}{R^3} + \frac{C(\eta,\zeta)}{R} \qquad (B.14)$$

Applying equation (11) to equation (B.13), it is obtained that

$$W_5(x,y,z) = -\frac{1}{\rho_\infty V_\infty}\int_{-\infty}^{x}\frac{\partial P_4}{\partial z}\,dx_1 \qquad (B.15)$$

It follows that

$$\frac{W_5(x,y,z)}{V_\infty(y,z)} = -\frac{1}{4\pi}\iiint C_p\cdot\left\{\frac{-C(z-\zeta)Y_t - 2\frac{M_\eta}{M}(y-\eta)(z-\zeta)}{Y_t^2}\left(1+\frac{x-\xi}{R}\right)\right.$$

$$\left. - \frac{\beta^2(x-\xi)\frac{M_\eta}{M}(y-\eta)(z-\zeta)}{Y_t\cdot R^3}\right\} d\xi\, d\eta\, d\zeta \qquad (B.16)$$

B.5 $$P_6 = -\frac{1}{4\pi\beta^2}\iiint \frac{M-\bar{M}^2}{R} P'_{\xi\xi}\, d\xi\, d\eta\, d\zeta \qquad (B.17)$$

By the divergence theorem

$$\iiint_V \nabla\cdot\vec{A}\; dv = \iint_{surface} \vec{A}\cdot\vec{n}\; ds \qquad (B.18)$$

$$\iiint \frac{P'_{\xi\xi}}{R}\, d\xi d\eta d\zeta = \iiint \left\{ \left(\nabla\cdot\vec{i}\ \frac{P'_\xi}{R} \right) - \frac{P'_\xi}{R^3} \right\} d\xi d\eta d\zeta \qquad (B.19)$$

Applying equation (B.18) to the first term on the right hand side of equation (B.19), it obtained that

$$\iiint \left(\nabla\cdot\vec{i}\ \frac{P'_\xi}{R} \right) dV = \iint \vec{i}\cdot\vec{n}\ \frac{P'_\xi}{R}\, dS = \iint_{\text{Wing Surface}} \frac{P'_\xi}{R}\, d\eta d\zeta \cong 0$$

Therefore, equation (B.17) becomes

$$P_6 = \frac{1}{4\pi\beta^2} \iiint \frac{3\beta^2 (z-\zeta)(x-\xi)(M^2-\bar{M}^2) P'_\xi}{R^5}\, d\xi d\eta d\zeta \qquad (B.20)$$

From equation (11), it can be shown that

$$W_6 = -\frac{1}{\rho_\infty V_\infty} \int_{-\infty}^{x} \frac{\partial P_5}{\partial z}\, dx_1$$

$$= -\frac{1}{4\pi\rho_\infty V_\infty} \iiint \frac{(z-\zeta)(M^2-\bar{M}^2) P'_\xi}{R^3}\, d\xi d\eta d\zeta \qquad (B.21)$$

It follows that

$$\frac{W_6(x,y,z)}{V_\infty(y,z)} = -\frac{1}{8\pi} \iiint \frac{(z-\zeta)(M^2-\bar{M}^2) C_{P_\xi}}{R^3}\, d\xi d\eta d\zeta \qquad (B.22)$$

B.6 Surface integrals in equations (14) and (15).

Following the quasi-vortex-lattice method (ref. 9), it is assumed that the velocity is constant for each spanwise vortex strip on the wing. Performing the integration along the bound element of each strip (Figure 4), the double integrals can be reduced to finite sums through the mid-point trapezoidal rule. Let

$$X - \xi = X - X_1 - \tau\ (X_2 - X_1)$$

$$Y - \eta = Y - Y_1 - \tau\ (Y_2 - Y_1)$$

$$R_\beta^2 = (X-\xi)^2 + \beta^2 (Y-\eta)^2 + \beta^2 Z^2$$

$$= \tau^2 \bar{A} + \tau \bar{B} + \bar{C}$$

where

$$\bar{A} = (X_2 - X_1)^2 + \beta^2 (Y_2 - Y_1)^2$$

$$\bar{B} = -2\left[(X - X_1)(X_2 - X_1) + \beta^2 (Y - Y_1)(Y_2 - Y_1)\right]$$

$$\bar{C} = (X - X_1)^2 + \beta^2 (Y - Y_1)^2 + \beta^2 Z^2$$

$$(Y-\eta)^2 + Z^2 = \tau^2 a + \tau b_1 + C_1$$

$$a = (Y_2 - Y_1)^2 \ , \quad b_1 = -2(Y - Y_1)(Y_2 - Y_1) \ , \quad C_1 = (Y - Y_1)^2 + Z^2$$

The second term on the right hand side of equation 15 can be written as

$$\overline{W}_2(X, Y, Z) = -\frac{\beta^2}{4\pi} \iint_{S_W} \frac{M_\xi(0)}{M} \frac{Z \cdot \Delta C_p(\xi, \eta)}{Y_2} \left(1 + \frac{X - \xi}{R_1}\right) d\xi\, d\eta \qquad (B.23)$$

Now, integrating equation (B.23) along the bound element of each vortex strip and assuming the Mach number is constant for each spanwise strip, it can be shown that

$$\overline{W}_2(X, Y, Z)$$

$$= \frac{-\Delta C_p \frac{M_\xi}{M}(0)}{4\pi} \Sigma \left\{ \int_0^1 \frac{Z(Y_2 - Y_1)\, d\tau}{a\tau^2 + b_1\tau + C_1} \right.$$

$$\left. + \int_0^1 \frac{Z(Y_2 - Y_1)\left[X - X_1 - \tau(X_2 - X_1)\right]}{a\tau^2 + b_1\tau + C_1 (\bar{A}\tau^2 + \bar{B}\tau + \bar{C})} d\tau \right\} \qquad (B.24)$$

where

$$\int_0^1 \frac{z(y_2 - y_1)\,d\tau}{a\tau^2 + b_1\tau + c_1}$$

$$= \frac{(y_2 - y_1)\,z}{|y_2 - y_1||z|}\left(\tan^{-1}\frac{2a + b_1}{2|(y_2 - y_1)z|} - \tan^{-1}\frac{b_1}{2|(y_2 - y_1)z|}\right) \qquad (B.25)$$

To integrate the second integral in equation (B.24), let

$$(y_2 - y_1)\tau - (y - y_1) = \bar{v}$$

$$\tau = 0 \qquad \bar{v} = -(y - y_1)$$

$$\tau = 1 \qquad \bar{v} = y_2 - y$$

$$a\tau^2 + b_1\tau + c_1 = \bar{v}^2 + z^2$$

$$\bar{A}\tau^2 + \bar{B}\tau + \bar{C} = \frac{1}{(y_2 - y_1)^2}\cdot(A'v^2 + 2B'\bar{v} + C') \qquad (B.26)$$

It follows that

$$\bar{F} = \int \frac{z(y_2 - y_1)}{v^2 + z^2}\cdot\frac{[x - x_1 - \tau(x_2 - x_1)]}{(A'v^2 + 2B'\bar{v} + C')^{1/2}}\,dv$$

$$= \left[-\tan^{-1}\frac{Q\bar{v} - (x_2 - x_1)z}{\sqrt{A'\bar{v}^2 + 2B'\bar{v} + C'}}\right]_{\bar{v} = y_1 - y}^{\bar{v} = y_2 - y} \qquad (B.27)$$

Using equations (B.25) and (B.27), equation (B.24) becomes

$$W_2(x, y, z) = \Sigma\left\{\frac{z}{|z|}\left(\tan^{-1}\frac{2a + b_1}{2|(y_2 - y_1)z|} - \tan^{-1}\frac{b_1}{2|(y_2 - y_1)z|}\right) + \bar{F}\right. \qquad (B.28)$$

where

$$A' = (x_2 - x_1)^2 + \beta^2(y_2 - y_1)^2$$

$$B' = [(x_2 - x_1)^2(y - y_1) - (x - x_1)(x_2 - x_1)(y_2 - y_1)]$$

$$C' = (x_2 - x_1)^2(y - y_1)^2 - 2(x - x_1)(x_2 - x_1)(y - y_1)(y_2 - y_1) + (x - x_1)^2(y_2 - y_1)^2 + \beta^2 z^2(y_2 - y_1)^2$$

$$Q = (x_2 - x_1)(y - y_1) - (x - x_1)(y_2 - y_1)$$

$$a = (y_2 - y_1)^2, \qquad b_1 = -2(y - y_1)(y_2 - y_1)$$

Finally, equation (B.28) becomes

$$\bar{W}_2(x,y,z) = \sum \left\{ \frac{z}{|z|} \left(\tan^{-1} \frac{y_2 - y}{|z|} - \tan^{-1} \frac{y_1 - y}{|z|} \right) + \bar{F} \right\} \quad (B.29)$$

The first term of equation (14) can be written as

$$C_{p_1}(x,y,z) = -\frac{1}{4\pi} \iint_{S_w} \frac{\beta^2 z \, \Delta C_p(\xi,\eta)}{R_1^3} d\xi \, d\eta \quad (B.30)$$

Following the steps used above, let

$$x - \xi = x - x_1 - \tau (x_2 - x_1)$$

$$y - \eta = y - y_1 - \tau (y_2 - y_1)$$

$$(x-\xi)^2 + \beta^2 (y-\eta)^2 + \beta^2 z^2 = \bar{A}\tau^2 + \bar{B}\tau + \bar{C}$$

Hence,

$$C_{p_1}(x,y,z) = -\frac{\beta^2 \Delta C_p}{4\pi} \cdot z \cdot (y_2 - y_1) \left[\frac{4\bar{A} + 2\bar{B}}{(4\bar{A}\bar{C} - \bar{B}^2)(\bar{A}+\bar{B}+\bar{C})^{1/2}} - \frac{2\bar{B}}{(4\bar{A}\bar{C} - \bar{B}^2)\bar{C}^{1/2}} \right] \quad (B.31)$$

where

$$\bar{A} = (x_2 - x_1)^2 + \beta^2 (y_2 - y_1)^2$$

$$\bar{B} = -2 \left[(x - x_1)(x_2 - x_1) + \beta^2 (y - y_1)(y_2 - y_1) \right]$$

$$\bar{C} = (x - x_1)^2 + \beta^2 (y - y_1)^2 + \beta^2 z^2$$

The second term on the right hand side of equation (14) is

$$C_{p_2}(x,y,z) = -\frac{1}{2\pi} \int_0^1 \frac{\frac{M_\infty}{M}(0) \, \Delta C_p (y_2 - y_1)}{(\bar{A}\tau^2 + \bar{B}\tau + \bar{C})^{1/2}} d\tau$$

$$= -\frac{1}{2\pi} \frac{M_\infty}{M}(0) \, \Delta C_p \frac{y_2 - y_1}{\bar{A}^{1/2}} \left[\sinh^{-1} \frac{2\bar{A} + \bar{B}}{(4\bar{A}\bar{C} - \bar{B}^2)^{1/2}} - \sinh^{-1} \frac{\bar{B}}{(4\bar{A}\bar{C} - \bar{B}^2)^{1/2}} \right] \quad (B.32)$$

APPENDIX C

Integration Regions and Coordinate Transformation

C.1 Integration regions and coordinate transformation in the ξ direction are indicated in Figures 6 and 7. For simplicity, denote the integrand by $F(\xi)$. Then,

$$\int_{-\infty}^{\infty} F(\xi)\,d\xi = \int_{-\infty}^{X_\ell} F(\xi)\,d\xi + \int_{X_\ell}^{X_t} F(\xi)\,d\xi + \int_{X_t}^{\infty} F(\xi)\,d\xi \qquad (C.1)$$

Note that the infinite regions are actually approximated by appropriate finite regions in numerical calculations. The upstream integral becomes

$$\int_{-\infty}^{X_\ell} F(\xi)\,d\xi \cong \int_{\pi/2}^{0} F(\theta)\,d\theta \qquad (C.2)$$

$$\xi = -X_a\,(1-\cos\theta) + X_\ell(J) \qquad \theta = \frac{K\pi}{2N_1}\,,\quad K=1,2,\cdots N_1$$

The second integral of equation (C.1) can be written as

$$\int_{X_\ell}^{X_t} F(\xi)\,d\xi = \int_{0}^{\pi} F(\theta_K)\,d\theta_K \qquad (C.3)$$

$$\xi_{1K} = X_{\ell_1} + C_1\,\xi_K \qquad \xi_{2K} = X_{\ell_2} + C_2\,\xi_K \qquad (C.3a)$$

$$\xi_K = \frac{1}{2}\,(1-\cos\theta_K) \qquad \theta_K = \frac{(2K-1)\,\pi}{2N_2} \qquad K=1,2,\cdots N_2$$

where

$$N_2 = 2^{N_P}\cdot\,(NW(1)+NW(2))$$

and

NW(1)+NW(2) = total aerodynamic panels on the wing in chordwise sections

Similarly, the downstream integral is reduced to

$$\int_{X_t}^{\infty} F(\xi)\,d\xi \cong \int_{0}^{\pi/2} F(\theta)\,d\theta \qquad (C.4)$$

$$\xi = X_t + X_b\,(1-\cos\theta)\,,\quad \theta = \frac{K\pi}{2N_3} \qquad K=1,2,\cdots N_3$$

C.2 Coordinate transformation in the spanwise direction

The integration regions and coordinate transformation are illustrated in Figure 6. If F(η) represents the integrand, then,

$$\int_{-\infty}^{\infty} F(\eta)d\eta = \int_{-\infty}^{-b/2} F(\eta)d\eta + \int_{-b/2}^{0} F(\eta)d\eta + \int_{0}^{b/2} F(\eta)d\eta + \int_{b/2}^{\infty} F(\eta)d\eta \qquad (C.5)$$

Again, infinite integration regions are approximated by finite regions in the numerical calculation.

The integration from $-\infty$ to the left wing tip can be reduced to

$$\int_{-\infty}^{-b/2} F(\eta)d\eta = -\int_{-b/2}^{-\infty} F(\eta)d\eta \cong -\int_{0}^{\pi/2} F(\phi)d\phi \qquad (C.6)$$

$$\eta = -b/2 - Y_S(1-\cos\phi)$$

$$\phi = \frac{K\pi}{2M_y} \qquad K = 1, 2, \cdots\cdots M_y$$

$$\phi = 0 \quad \eta = -b/2 \quad , \quad \phi = \pi/2 \quad \eta = -b/2 - Y_S$$

Note that M_y is the number of integration points outside the wing in the spanwise direction.

Integration points for the integration perfomed over the wing in the spanwise direction coincide with the ends point of the vortex strips. Therefore,

$$\eta = b/2\left(1-\cos\frac{(2j-1)\pi}{2N_S}\right)$$

On the other hand, the integration from the right wing tip to ∞ can be reduced to

$$\int_{b/2}^{\infty} F(\eta)d\eta \cong \int_{0}^{\pi/2} F(\phi)d\phi \qquad (C.7)$$

$$\eta = b/2 + y_s(1-\cos\phi) \qquad \phi = \frac{K\pi}{2M_y} \qquad K=1,2,\cdots M_y$$

$$\phi=0 \quad \eta=b/2 \;, \qquad \phi=\pi/2 \quad \eta=b/2+y_s$$

C.3 Integration in the vertical direction

Assume the integrand is $F(\zeta)$. Then

$$\int_{-\infty}^{\infty} F(\zeta)d\zeta = \int_{-\infty}^{0} F(\zeta)d\zeta + \int_{0}^{\infty} F(\zeta)d\zeta \qquad (C.8)$$

The integration from $\zeta=-\infty$ to $\zeta=0$ is reduced to

$$\int_{-\infty}^{0} F(\zeta)\,d\zeta \cong \int_{\pi/2}^{0} F(\psi)\,d\psi \qquad (C.9)$$

$$\zeta = -z_a(1-\cos\psi) \;, \quad \psi = \frac{K\pi}{2M_a} \qquad K=1,2,\cdots M_1$$

$$\psi=\pi/2 \quad \zeta=-z_a \;, \quad \psi=0 \quad \zeta=0$$

where M_a is the number of integration points in the z direction.

On the other hand, the integration from $\zeta=0$ to $\zeta=\infty$ becomes

$$\int_{0}^{\infty} F(\zeta)d\zeta \cong \int_{0}^{\pi/2} F(\psi)d\psi \qquad (C.10)$$

$$\zeta = z_b(1-\cos\psi) \;, \quad \psi = \frac{K\pi}{2M_b} \;, \; K=1,2,\cdots M_2$$

$$\psi=0 \quad \zeta=0 \;, \quad \psi=\pi/2 \quad \zeta=z_b$$

where M_b is the number of integration points in the positive Z direction.

APPENDIX D

Calculation of Wing Wake

Silverstein and Katzoff (ref. 14 and ref. 15) obtained empirical equations for calculating the wing wake. The maximum loss of dynamic pressure in the wake q_m can be expressed as following equation.

$$\frac{q_m}{q_u} = \frac{2.42\, C_d^{0.5}}{\frac{x}{c} + 0.3} \qquad (D-1)$$

where C_d is the wing section profile-drag coefficient, and x is the distance between wing trailing edge to the aerodynamic center of the tail. q_u represents the dynamic pressure of the uniform portion of the wake flow profile. The distribution of the dynamic pressure loss within the wake is q :

$$\frac{q}{q_m} = \cos^2\left(\frac{\pi}{2} \cdot \frac{\zeta}{b}\right) \qquad (D-2)$$

The half width b of the wake is given by

$$\frac{b}{c} = 0.68 \cdot C_d^{0.5} \left(\frac{x}{c} + 0.15\right)^{0.5} \qquad (D-3)$$

From Equations (D-1), (D-2), a function of the Mach number profile of the wing wake can be shown as the following expression.

$$M(\zeta) = M_1 \left[1 - \frac{2.42\, C_d^{0.5}}{\frac{x}{c} + 0.3} \cos^2\left(\frac{\pi \zeta}{2b}\right)\right]^{1/2} \qquad (D-4)$$

The wake location can be determined by using the method of Chapter 7 of reference 16. Assuming elliptic circulation distribution for wing in the spanwise direction, then the induced angle of attack is given as:

$$\alpha_i = C_L/\pi AR \qquad (D\text{-}5)$$

where experimental data for C_L are to be used (ref. 16).

The downwash angle ε_i can be obtained from figure 7-14 (ref.16) by using α_i. Finally, the downward displacement of the wake can be approximated by the following equation:

$$Z_w = \bar{Z} + \int_{T.E}^{l\cos(\theta-\alpha)} \tan\varepsilon\, dx \approx \bar{z} + \sum_i \Delta x \cdot \tan\varepsilon_i \qquad (D\text{-}6)$$

where $Z \approx 0.75\sin\alpha$ for angle of attack without flow seperation.

$Z \approx 0.75\sin(\alpha - \varepsilon_i)$ for angle of attack with flow seperation.

Table 1. Convergence Check of Numerical Integration for Joukowski Airfoil

CASE NO.	IGP	X_a	X_b	Z_a	Z_b	N1	N2	N3	M_a	M_b
1	5	9.0	8.0	3.0	3.0	20	10	10	10	10
2	5	9.0	8.0	3.0	3.0	15	10	10	10	10
3	5	9.0	8.0	3.0	3.0	10	10	10	10	10
4	5	9.0	8.0	3.0	3.0	5	10	5	5	5
5	5	9.0	8.0	2.0	2.0	15	10	10	5	5
6	5	9.0	8.0	2.0	2.0	10	10	10	5	5
7	5	12.0	11.0	2.0	2.0	20	10	20	5	5
8	1	9.0	8.0	3.0	3.0	20	10	10	10	10
9	1	9.0	8.0	3.0	2.0	10	10	10	5	5

Case No. \ I	1	2	3	4	5	6	7	8	9	10
1	0.7259	1.3235	2.0064	2.5672	2.9164	2.9887	2.7457	2.182	1.3123	0.1090
2	0.7488	1.3310	2.0108	2.5702	2.9185	2.9902	2.7468	2.1830	1.3128	0.1091
3	0.8061	1.3498	2.0217	2.5777	2.9239	2.9942	2.7496	2.1850	1.3139	0.1095
4	1.7472	1.6748	2.2311	2.7397	3.0578	3.1057	2.8391	2.2491	1.3509	0.1214
5	0.6686	1.3113	2.0082	2.5768	2.9309	3.0042	2.7613	2.1940	1.3186	0.1109
6	0.7253	1.3302	2.0196	2.5845	2.9365	3.0083	2.7643	2.1960	1.3198	0.1127
7	0.8506	1.3701	2.0413	2.5982	2.9456	3.0144	2.7683	2.1985	1.3212	0.1190
8	0.7294	1.3249	2.0075	2.5683	2.9174	2.9896	2.7465	2.1863	1.3126	0.1091
9	0.7363	1.3345	2.0228	2.5875	2.9392	3.0110	2.7664	2.1976	1.3207	0.1116

Notes. I indicates the pressure point locations given by Eq. (C.3a).

Case 1 is judged to be the best solution.

IGP=5:by least square method with 100 points of Z_v in equation (12)

IGP=1: with Z_v=0.05 only in equation (12)

Airfoil chord length=1.0

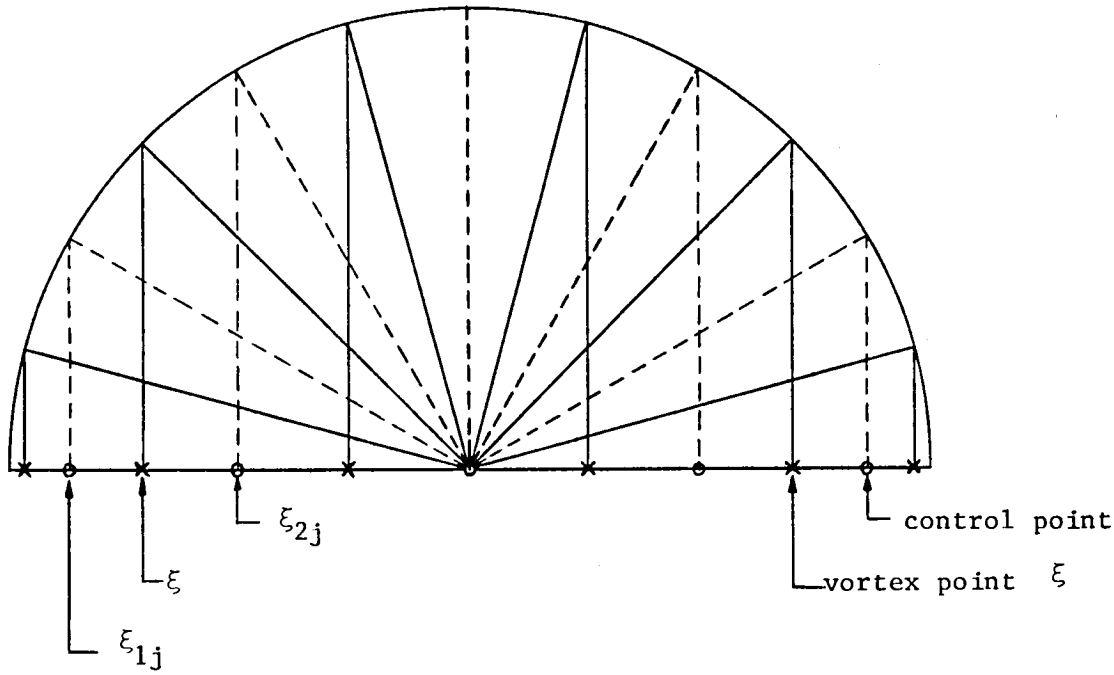

Figure 1. Parameters in the Assumed Pressure Function for Two-Dimensional Flow

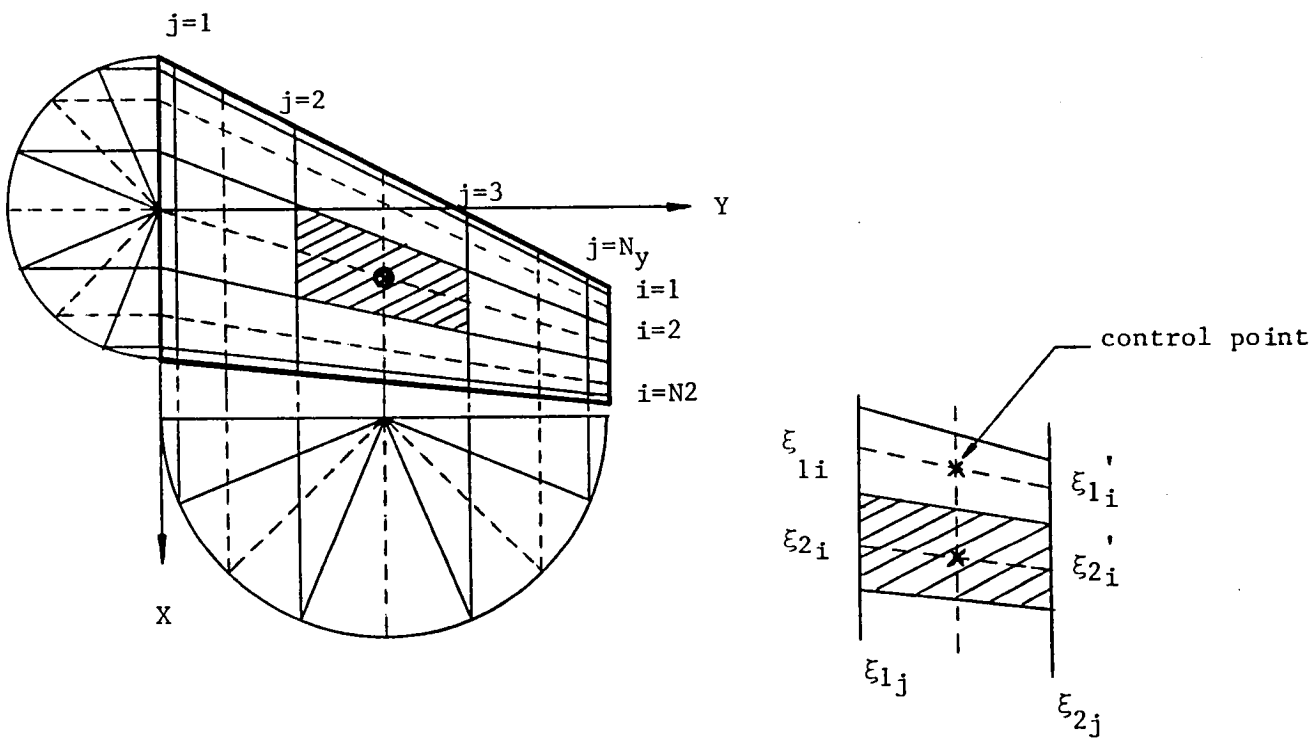

Figure 2. Parameters in the Assumed Pressure Function for Three-Dimensional Flow

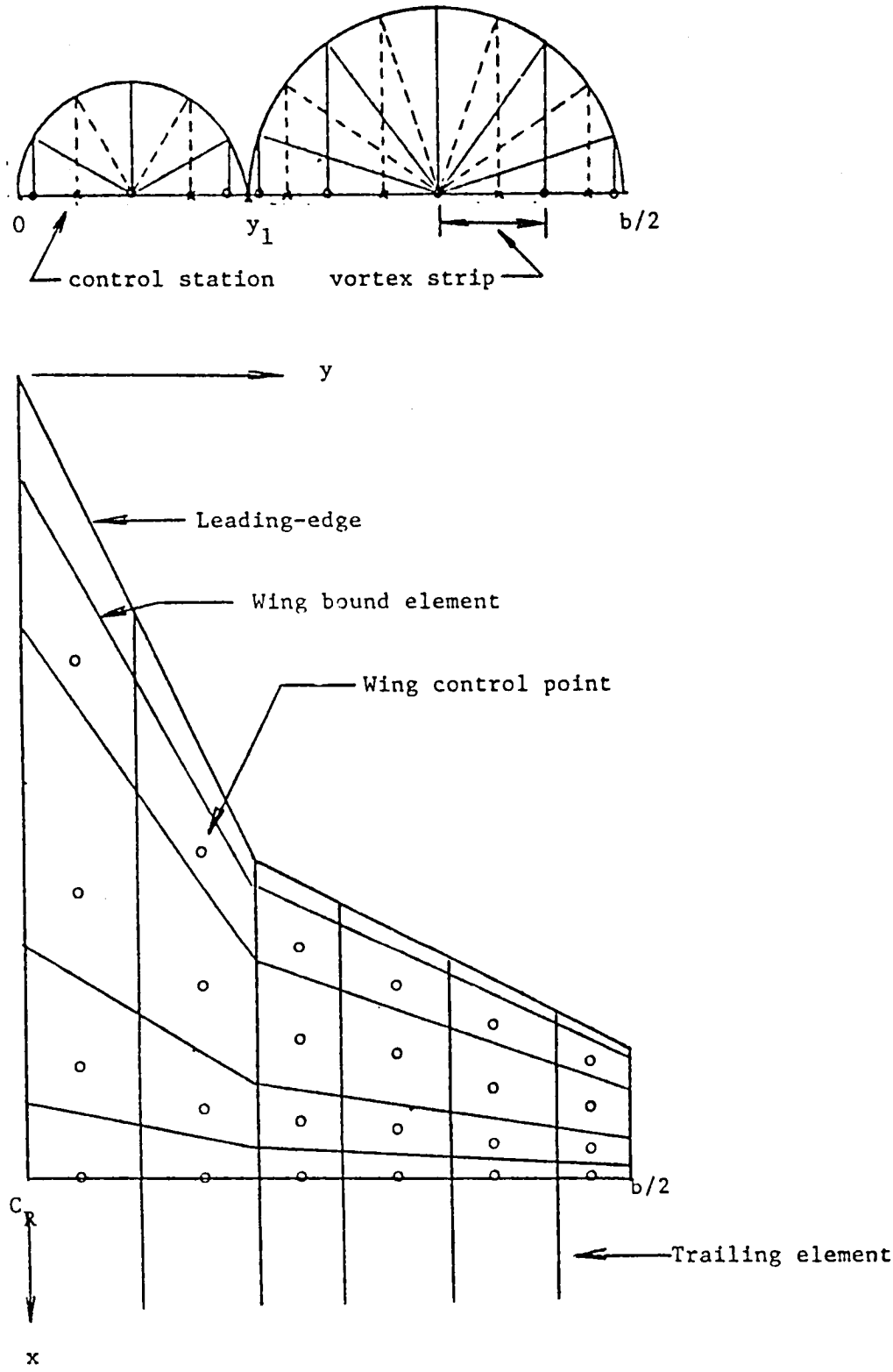

Figure 3. Vortex Element and Control Point Distribution Over the Wing

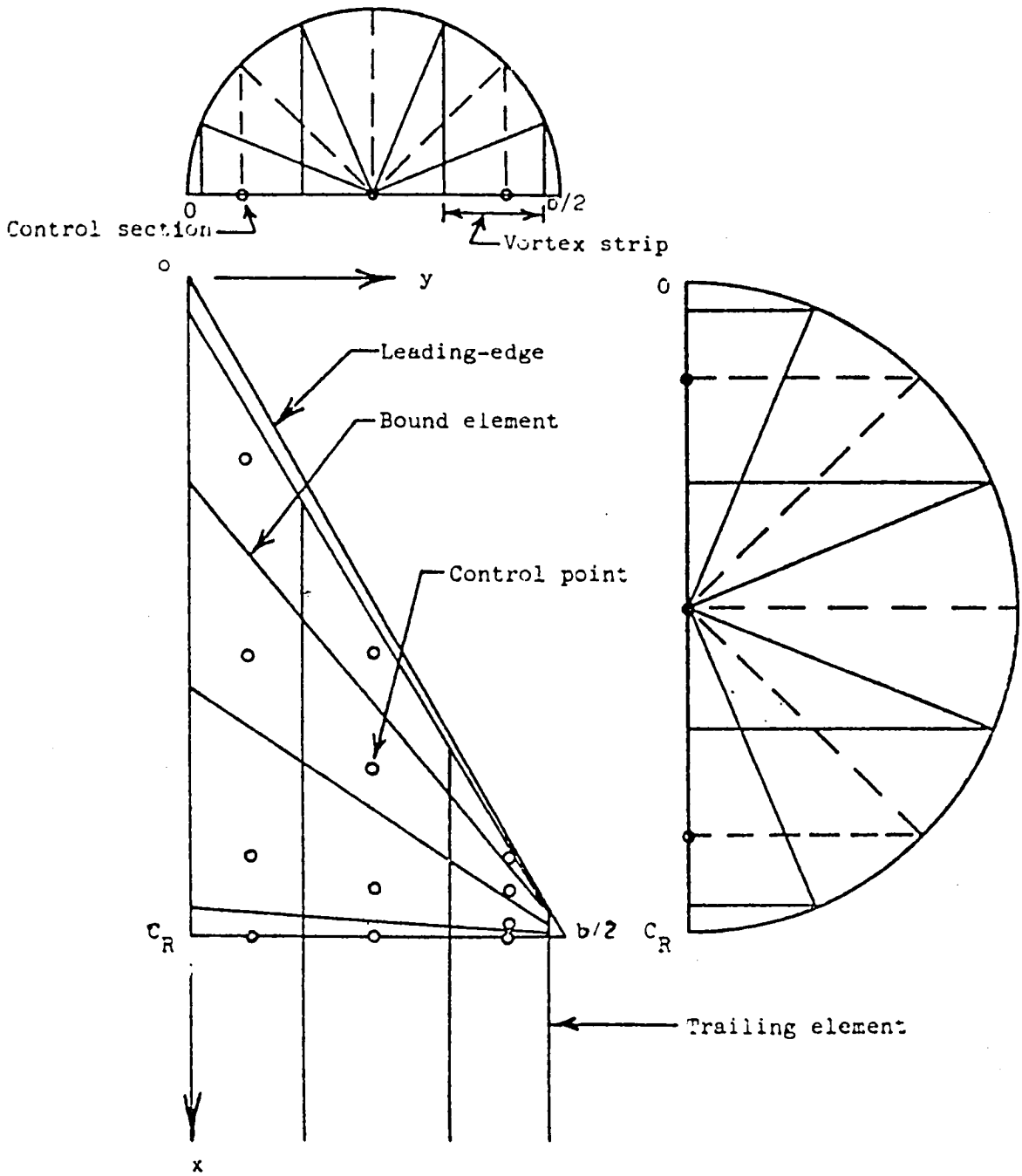

Figure 3. Continued

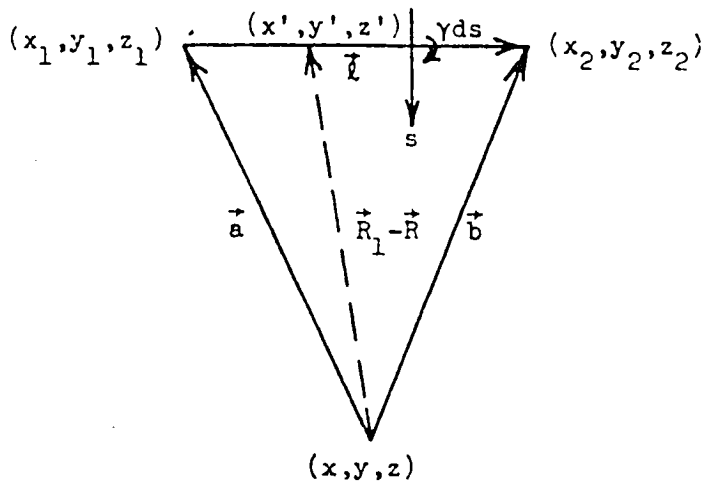

Figure 4. - Vortex Segment Geometry

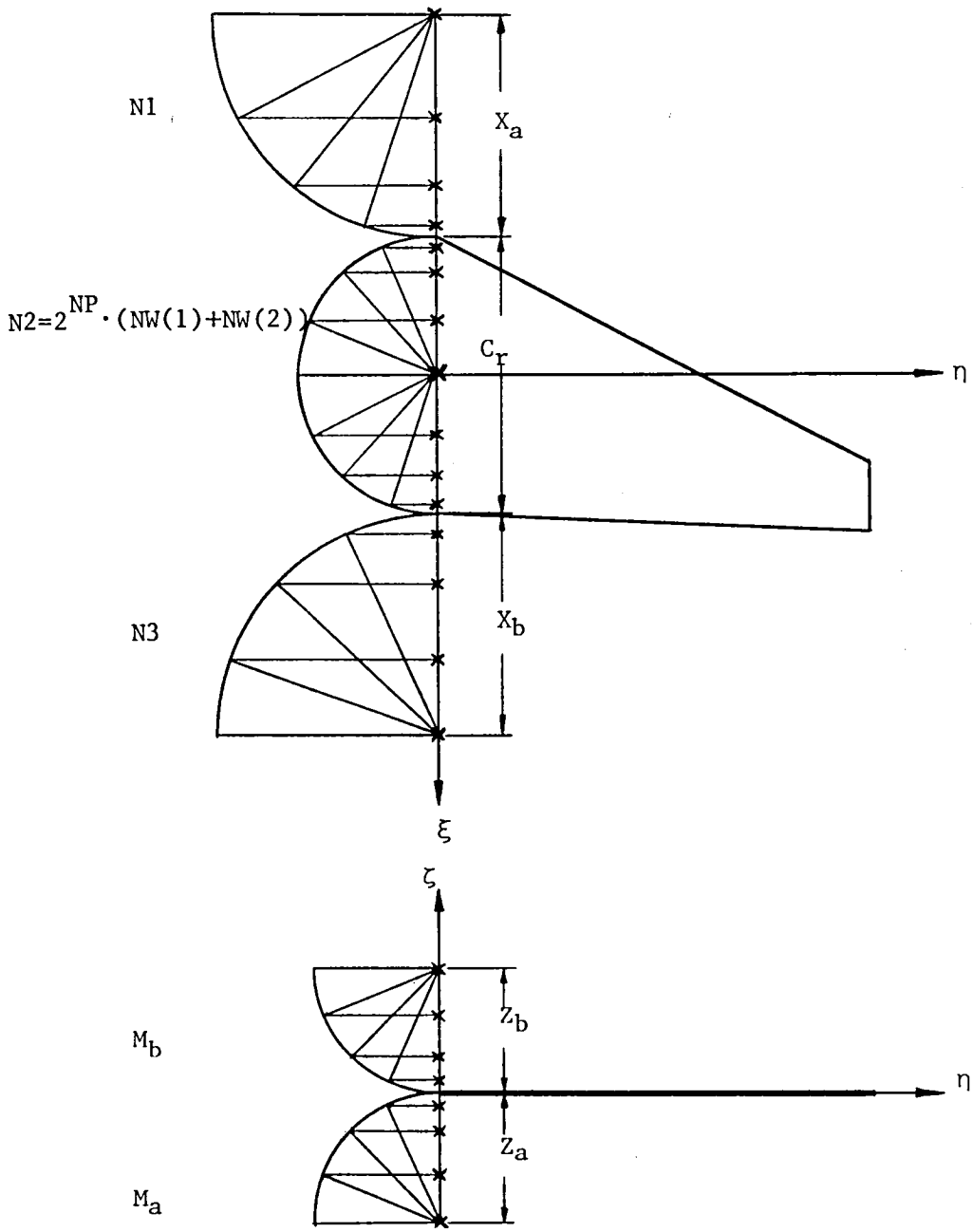

Figure 5. Integration Points and Region in Chordwise and Vertical Direction

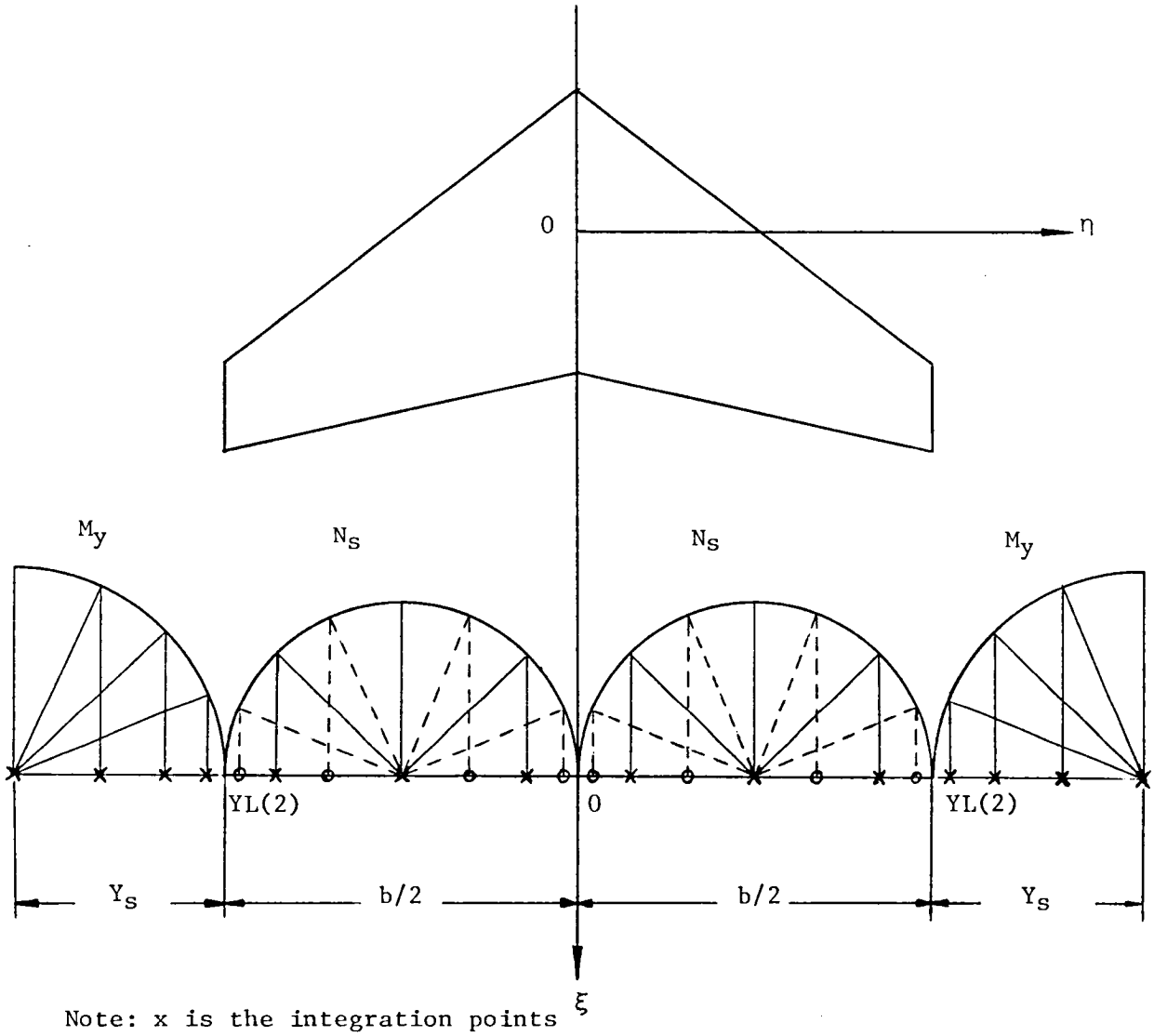

Note: x is the integration points

Figure 6. Integration Points and Regions in the Spanwise Direction

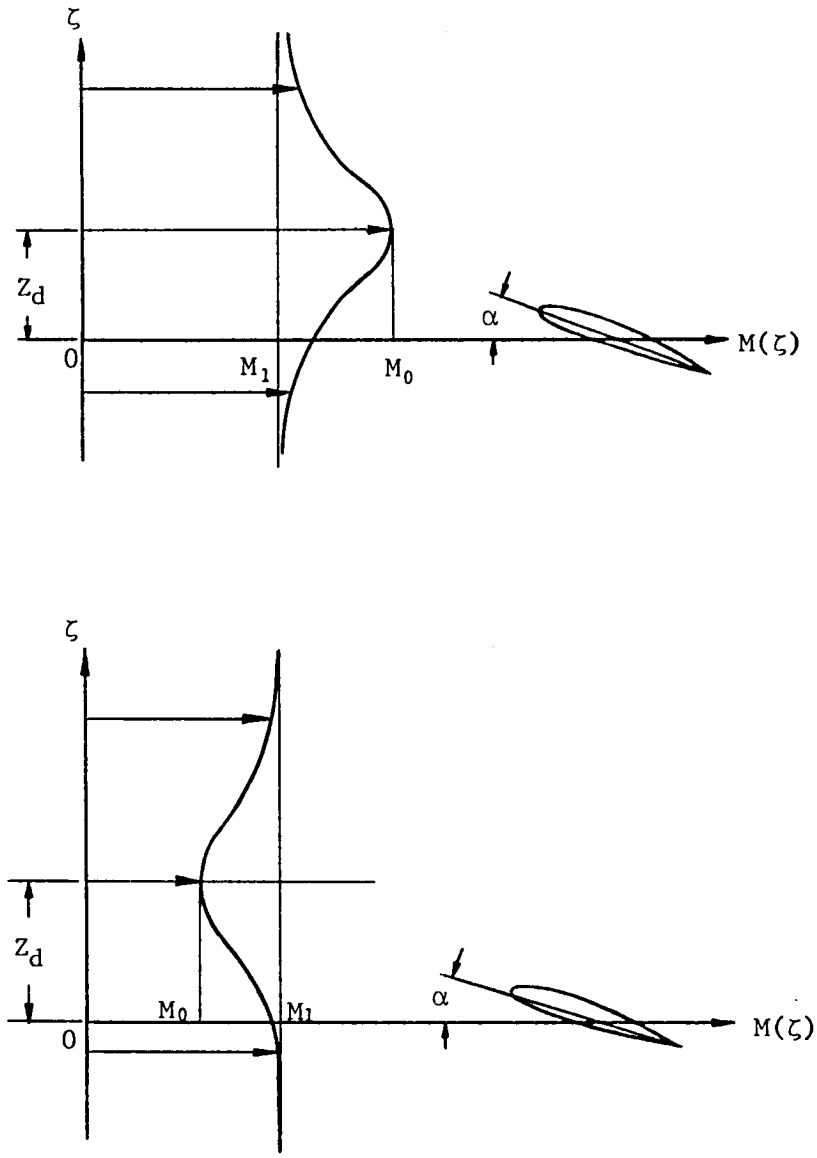

Figure 7. Mach number profile for jet and wake streams

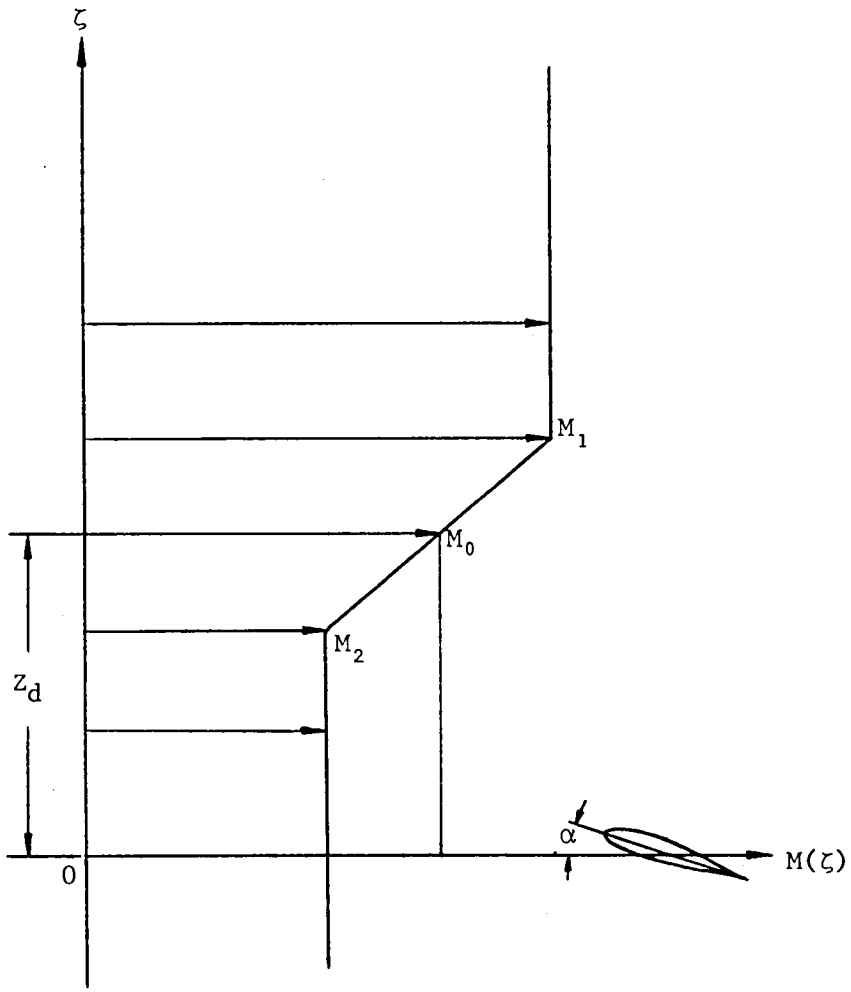

Figure 8. Mach number profile for a linear shear stream

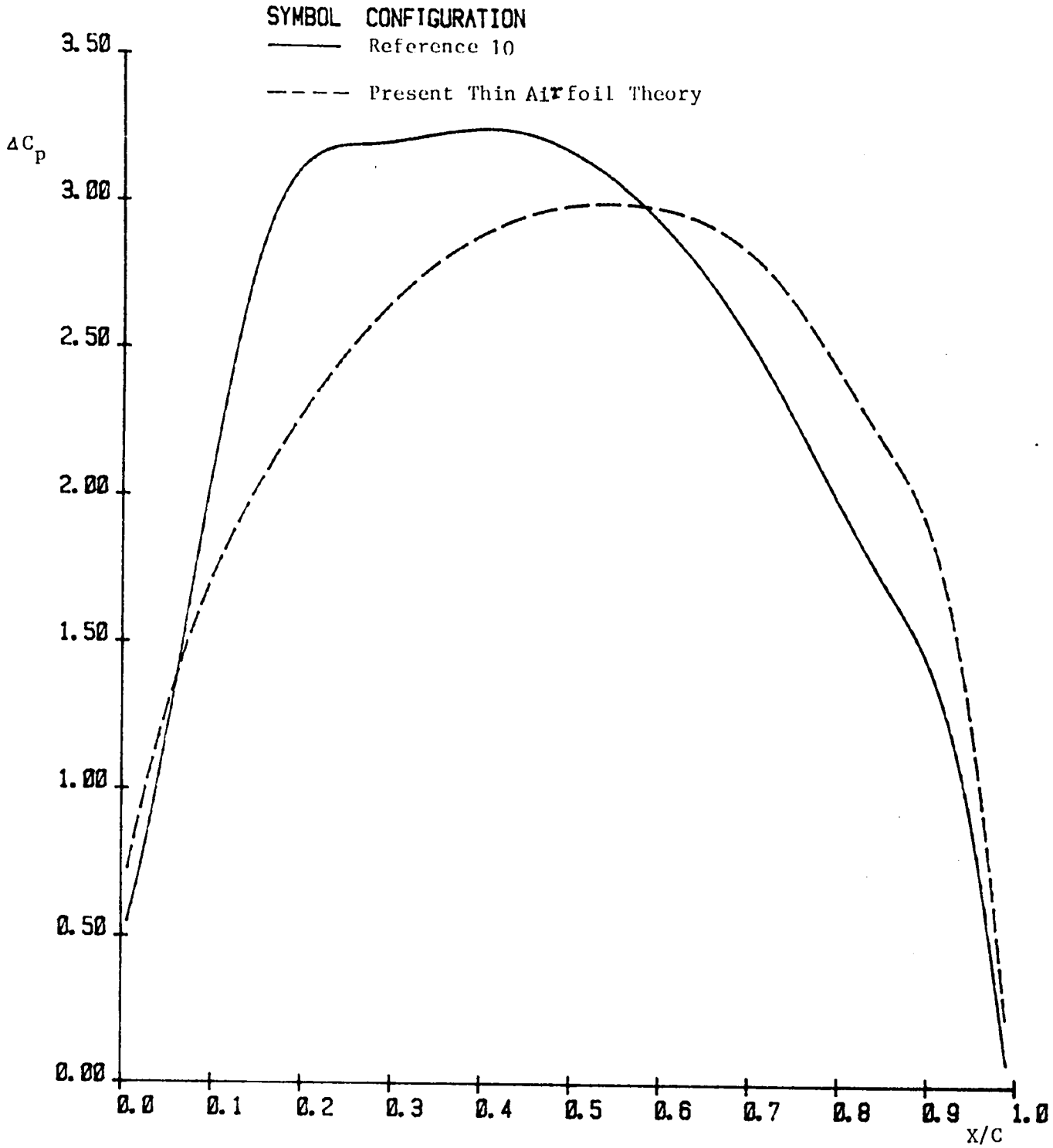

Figure 9. Pressure Difference Distribution on Joukowski Airfoil at $\alpha=0^{o}$ in Nonuniform Flow

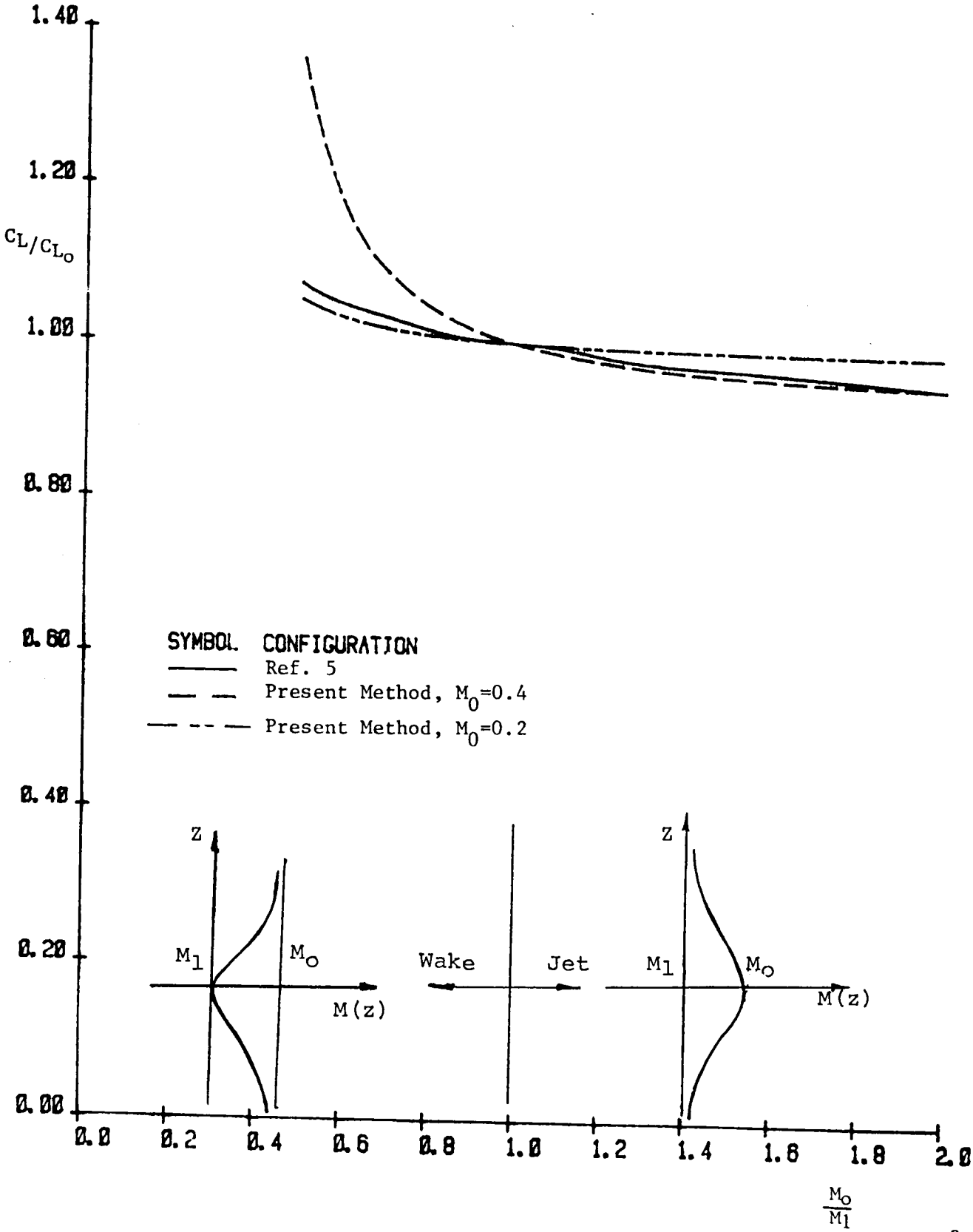

Figure 10. Lift Coefficient Ratio for an Elliptic Wing of $AR=10./(1-M_o^2)^{1/2}$ in Nonuniform Flow. C_{L_o} is the Lift Coefficient in Uniform Flow. Reference Dynamic Pressure= $0.5\rho(0)V(0)^2$

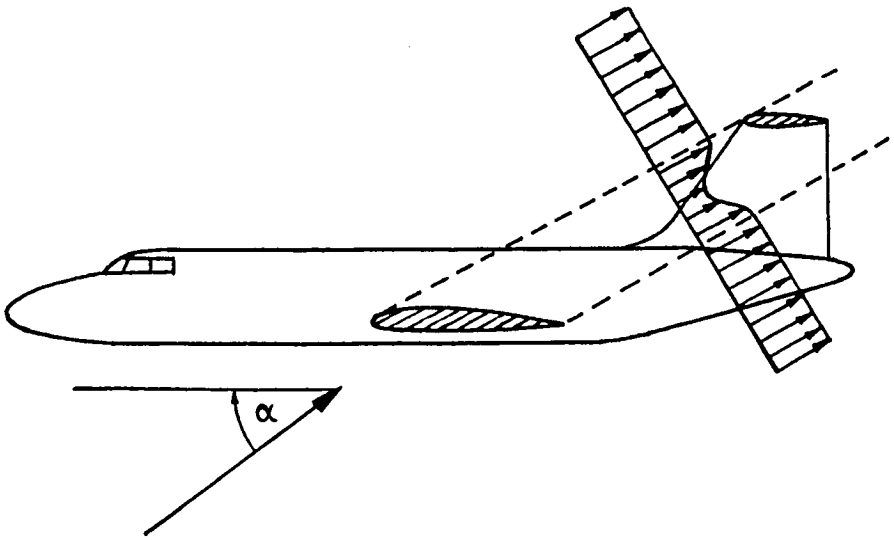

(a)

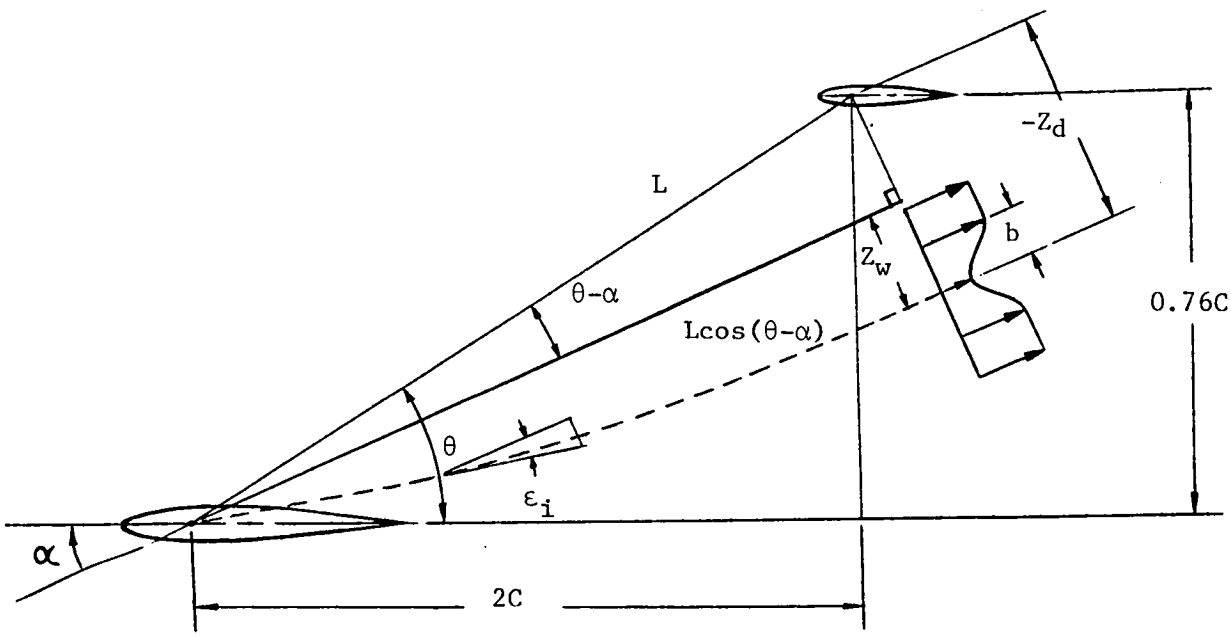

(b)

Figure 11. Wake of the Wing at High Angles of Attack

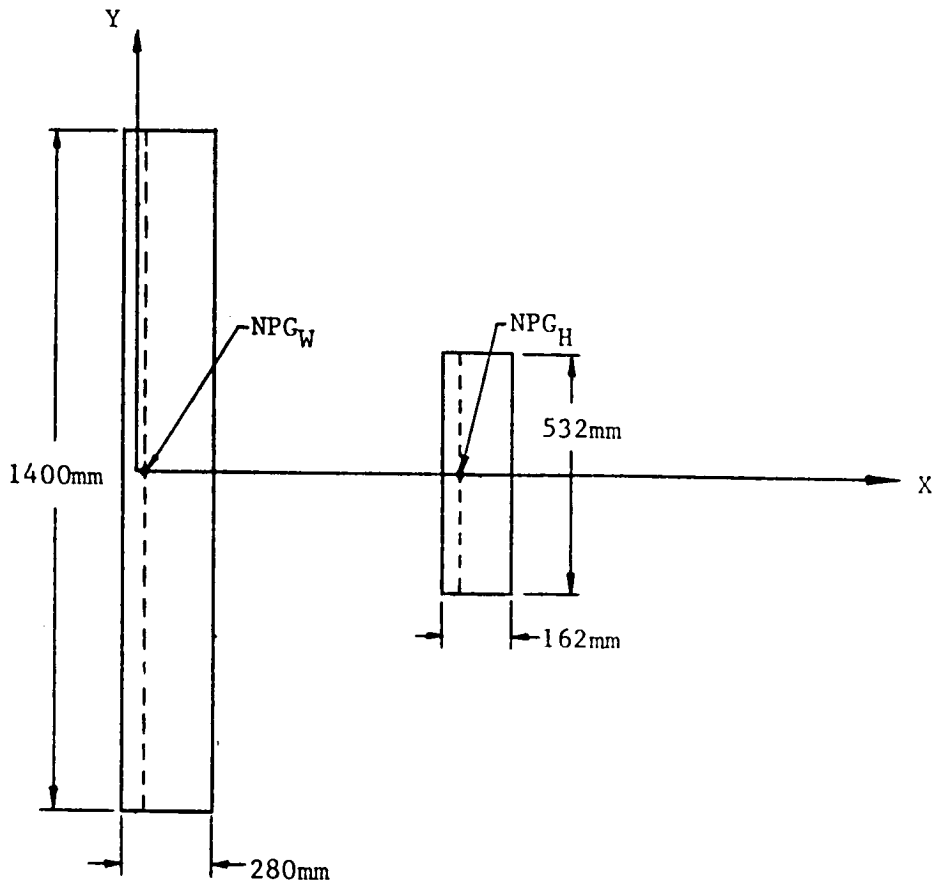

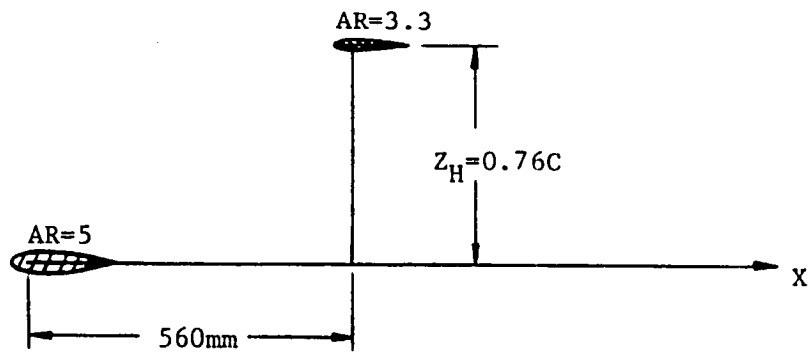

NPG: Geometry Neutralpoint, $\frac{X_{NPG}}{\bar{c}_{o_{wing}}}=0.25$, $\frac{X_{NPG_H}}{\bar{c}_{o_{tail}}}=0.25$

Figure 12. Geometry of Wing-Flat Horizontal Tail

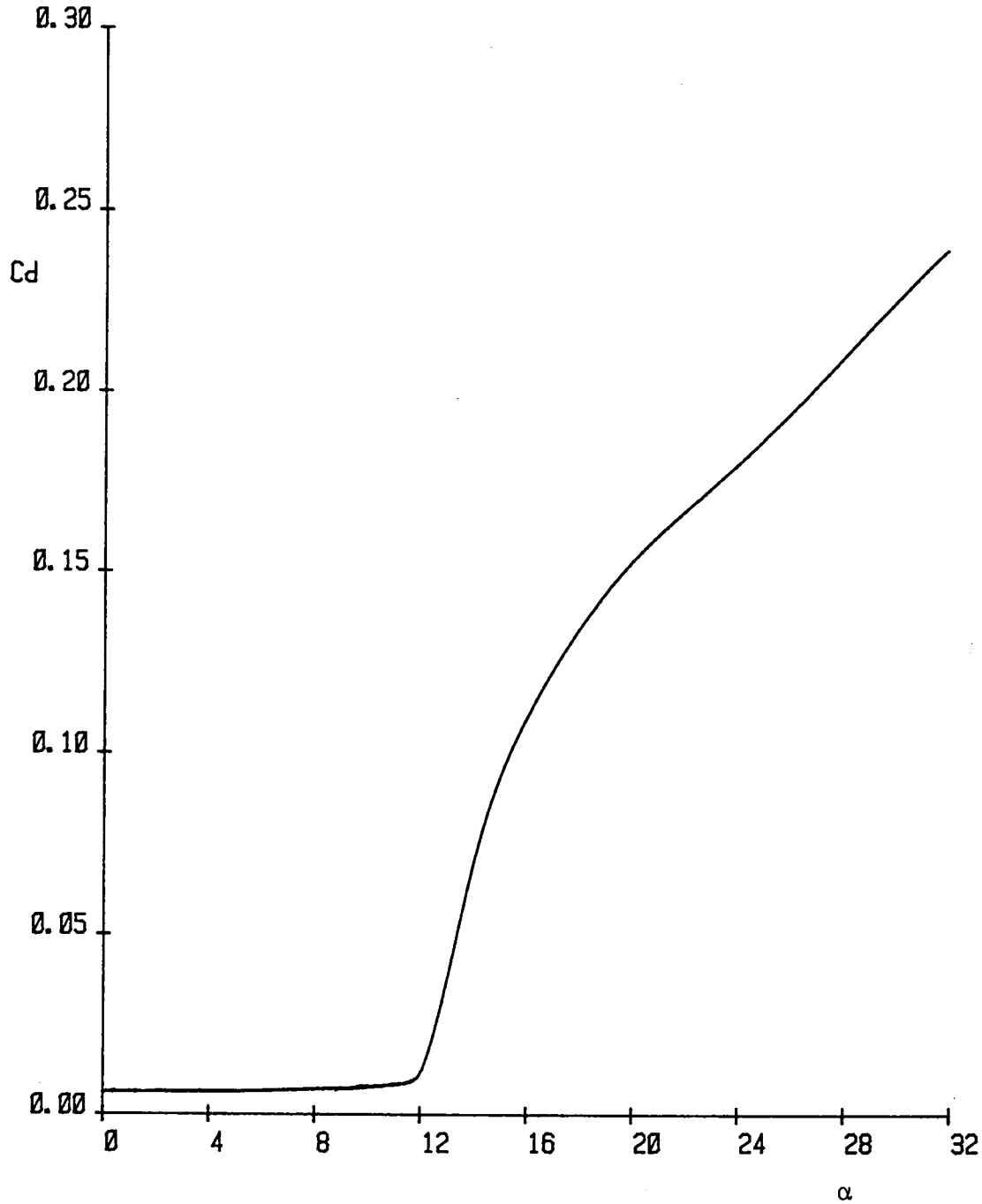

Figure 13. Assumed Cd of Wing Section Versus WIng Angle of Attack

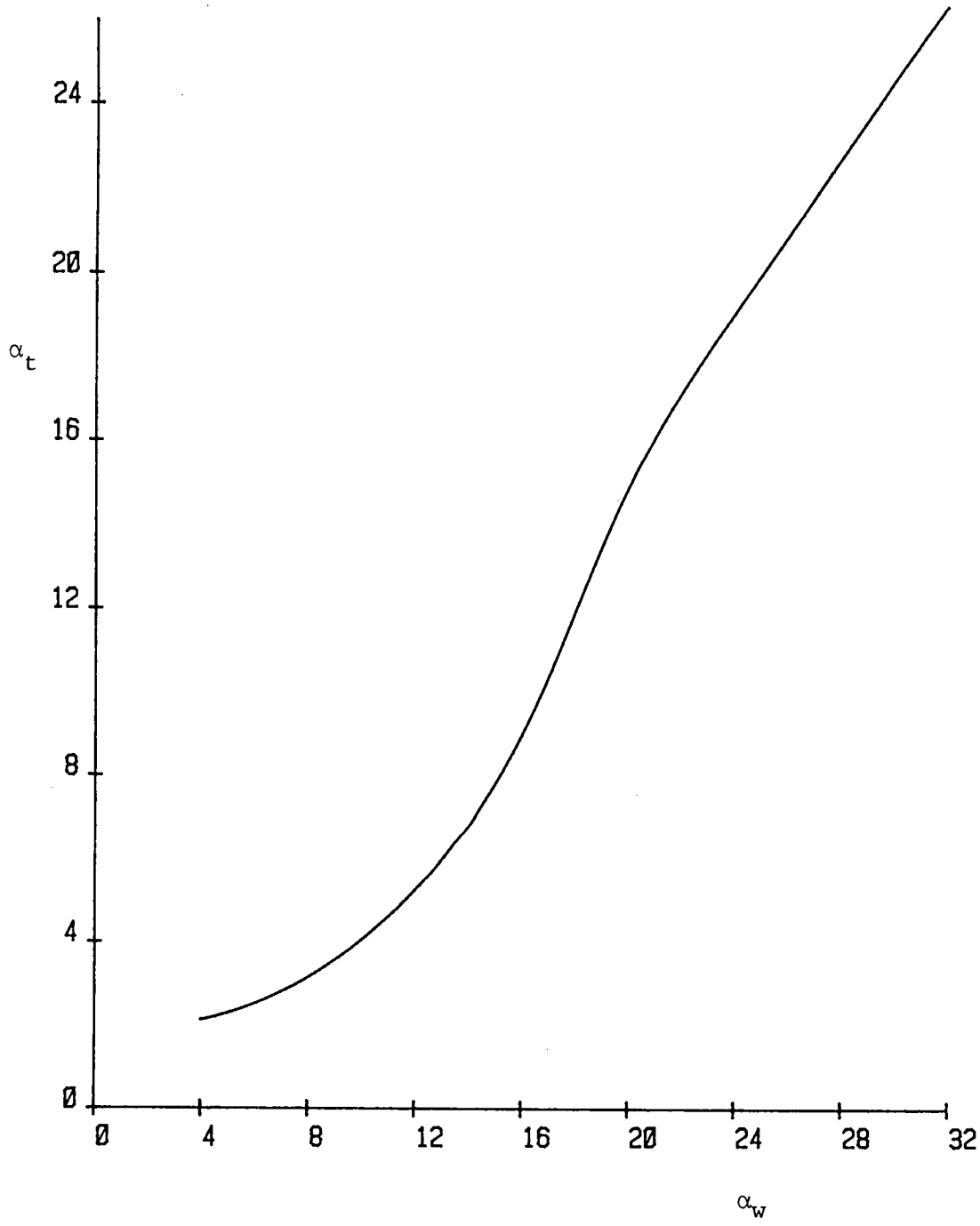

Figure 14. Wing Angle of Attack Versus Tail Angle of Attack

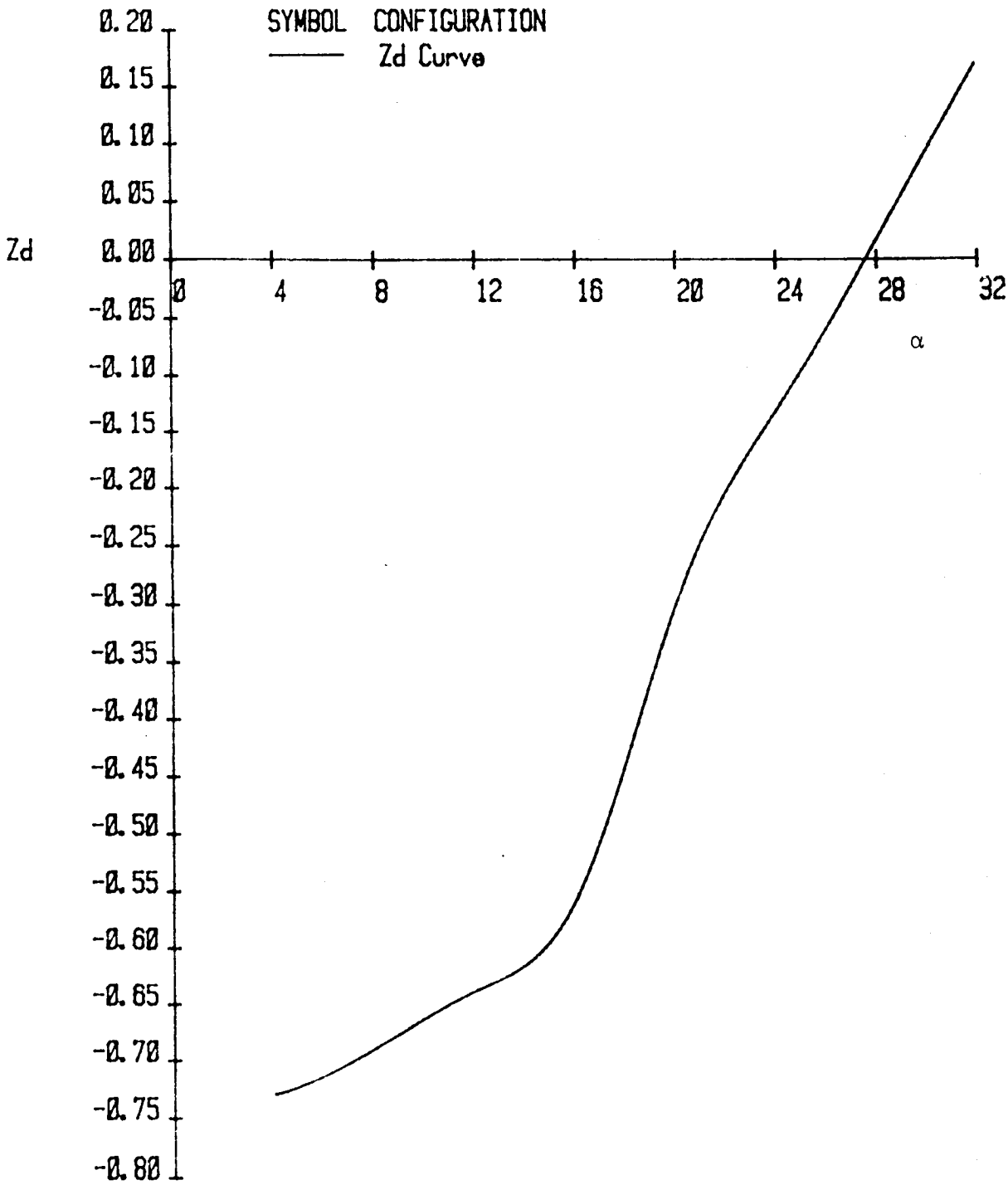

Figure 15. Zd Versus Wing Angle of Attack

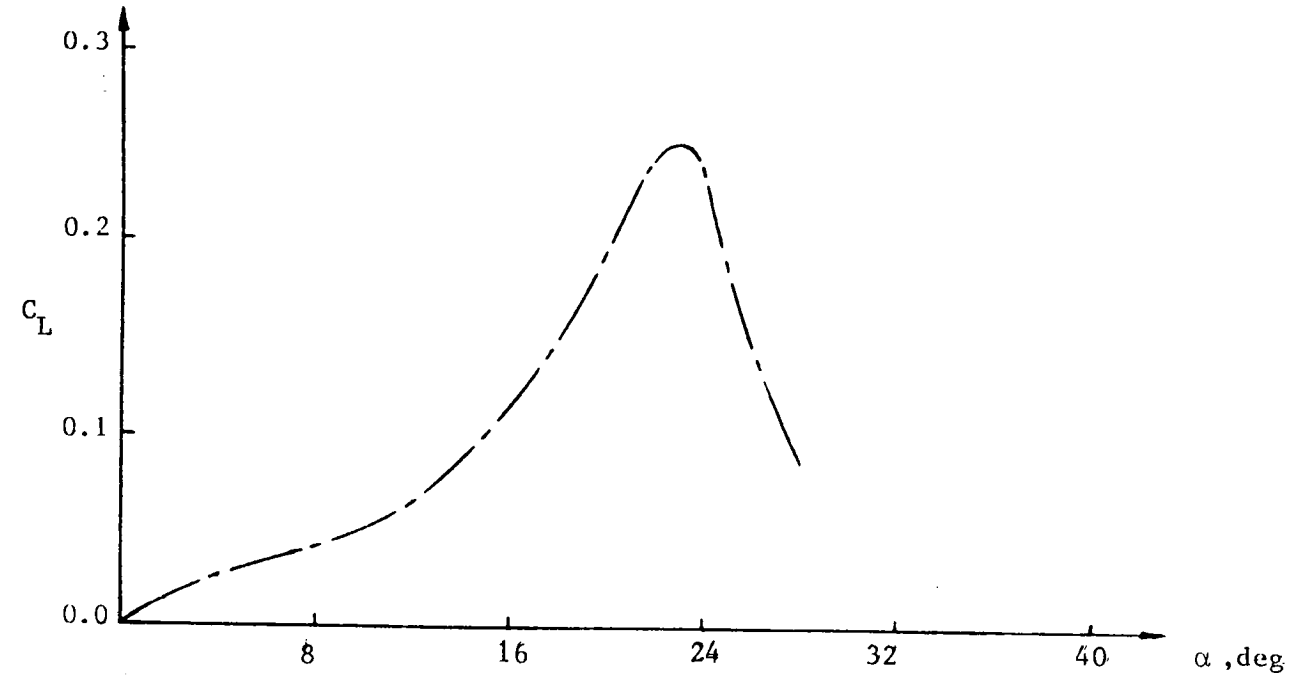

(a) C_L Versus α

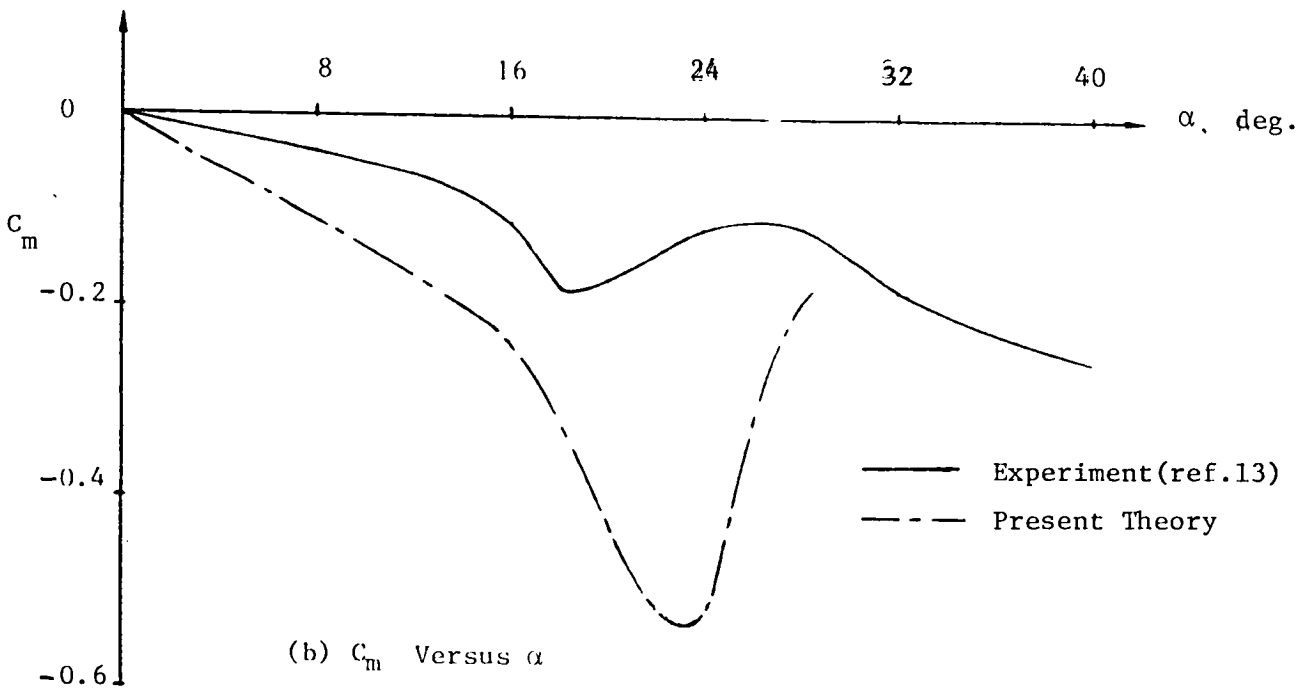

(b) C_m Versus α

Reference Moment point at y axis

Figure 16. Aerodynamic Characteristics of Plane Tail (AR=3.3) Due to Wing Wake Effect

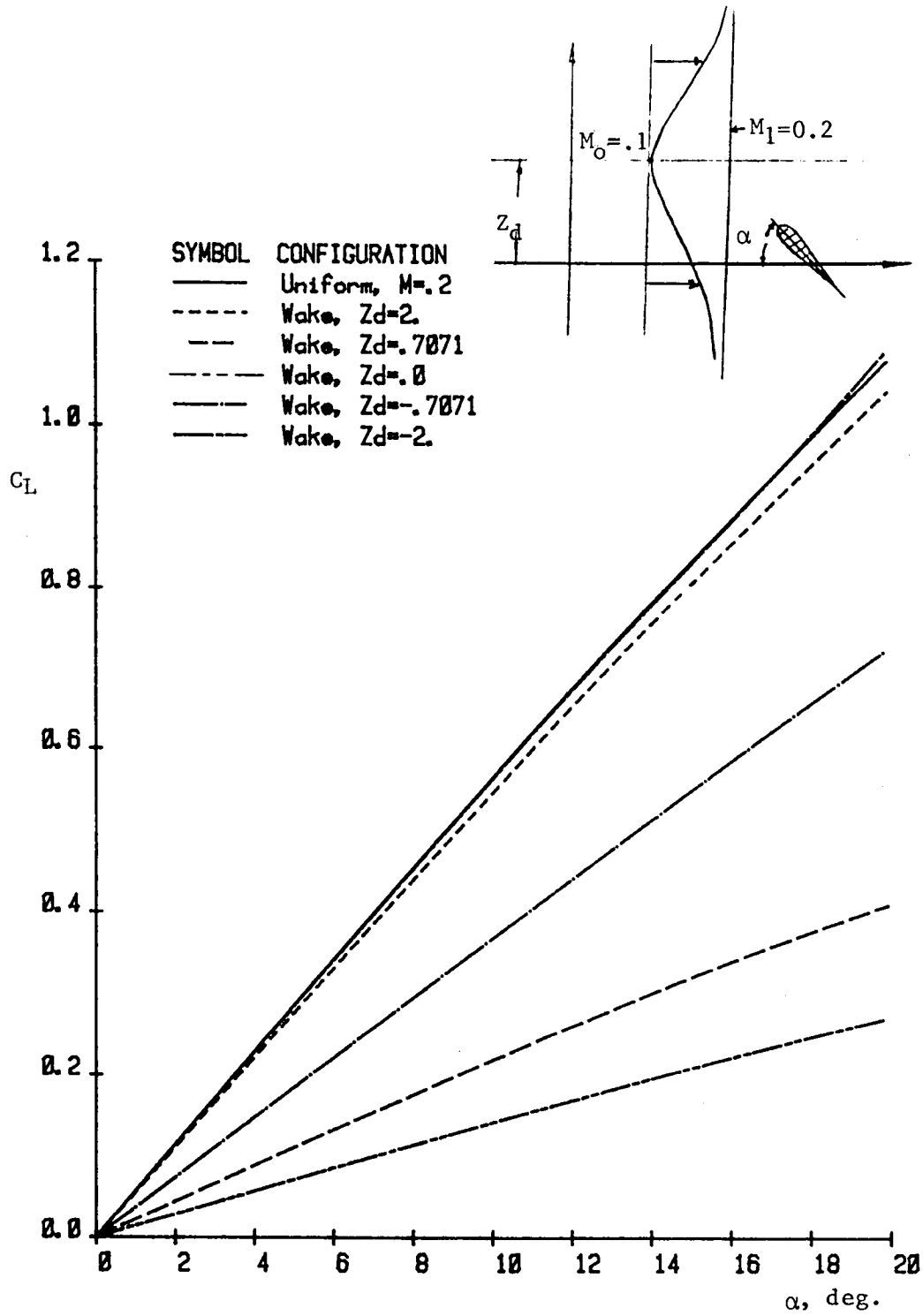

(a) C_L Versus α

Figure 17. Longitudinal Aerodynamic Characteristics of Flat Rectangular Wing (AR=3.3) in the Wake, Reference Dynamic Pressure = $0.5\ \rho_1 V_1^2$

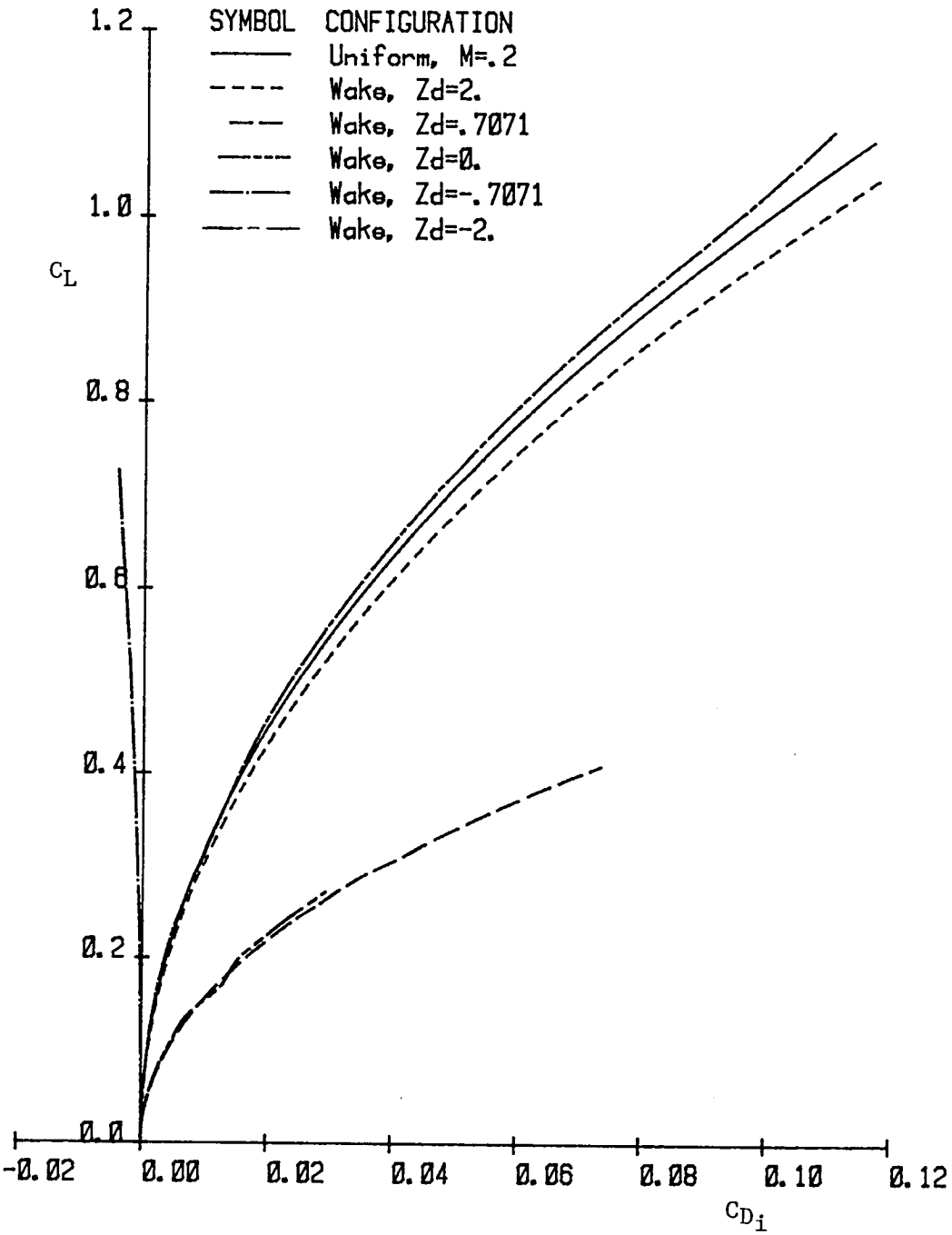

(b) C_L Versus C_{D_i}

Figure 17. Continue

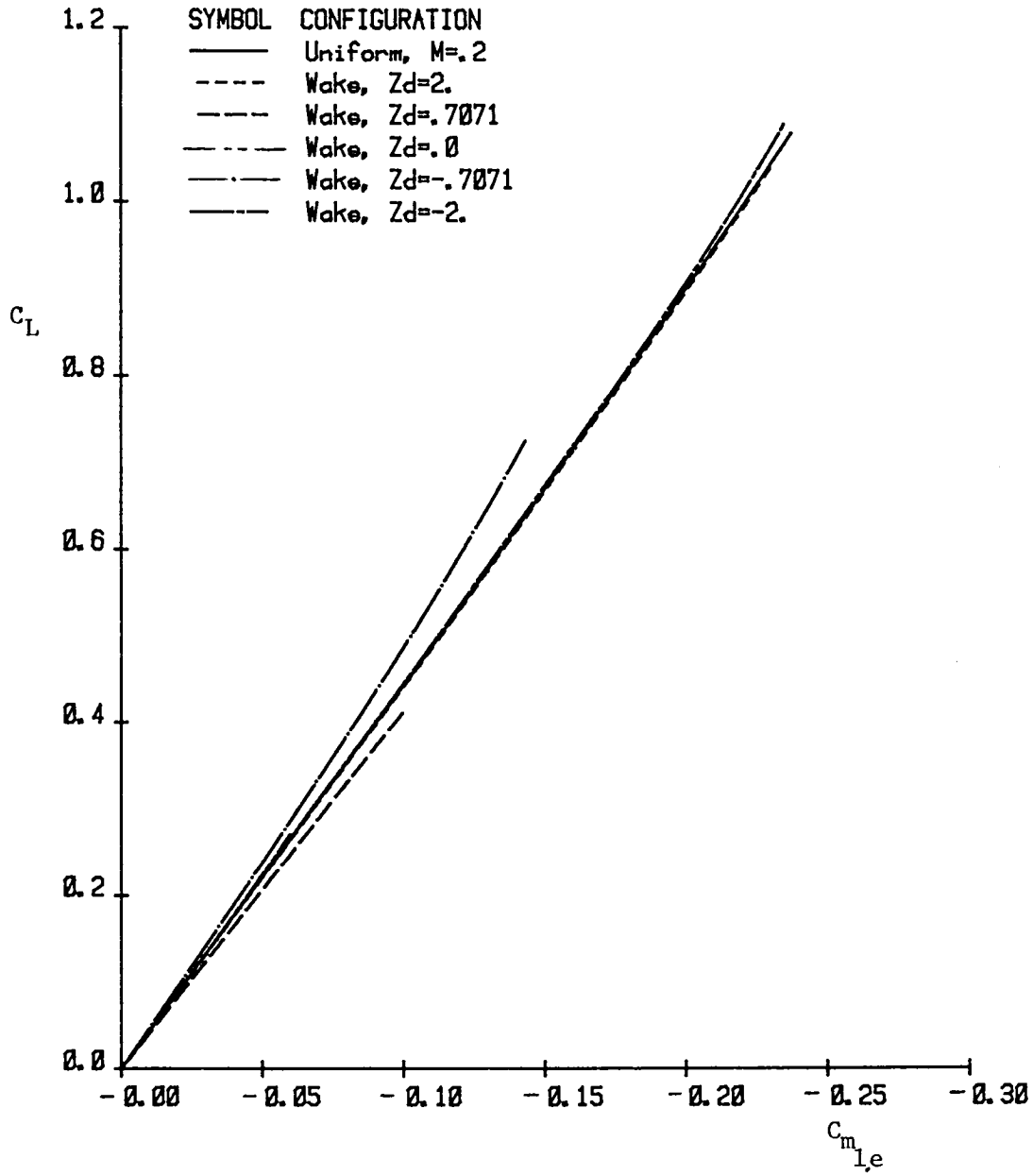

(C) C_L Versus C_m

Figure 17. Continued

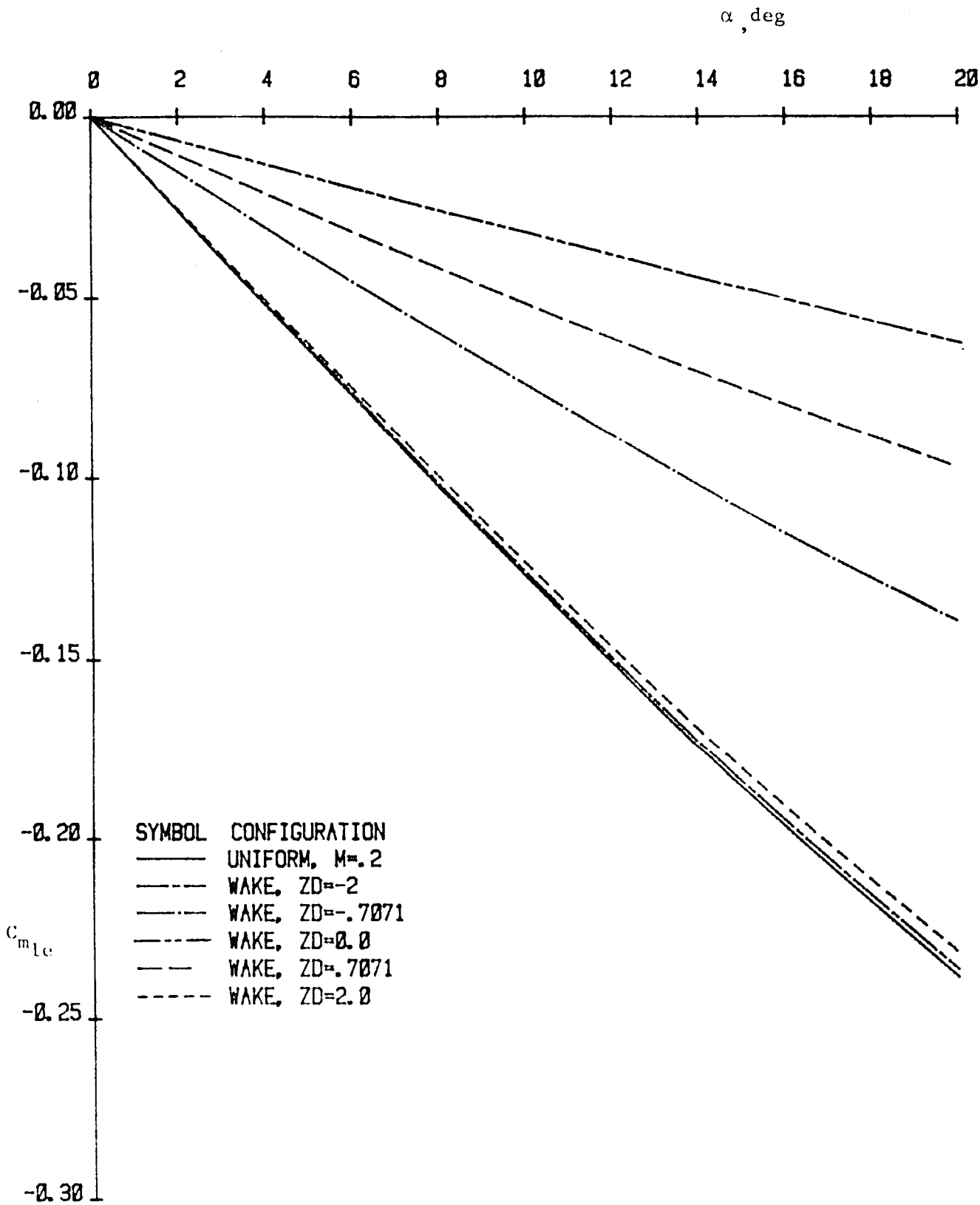

(d) C_m Versus α

Figure 17. Concluded

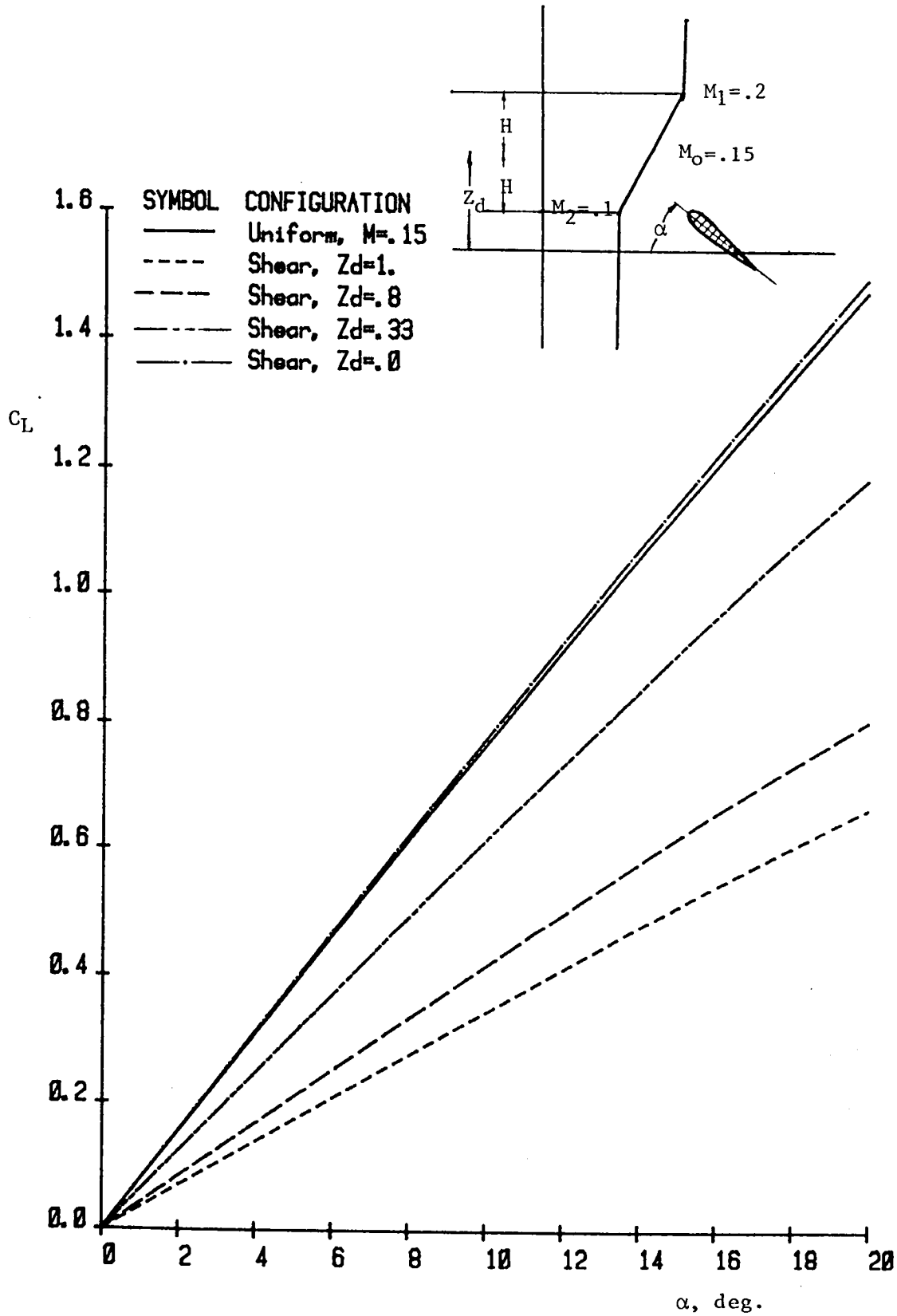

(a) C_L Versus α

Figure 18. Longitudinal Aerodynamic Characteristics of Flat Rectangular Wing (AR=7.2) in Shear Flow. Reference Dynamic Pressure= 0.5 $\rho_1 V_1^2$

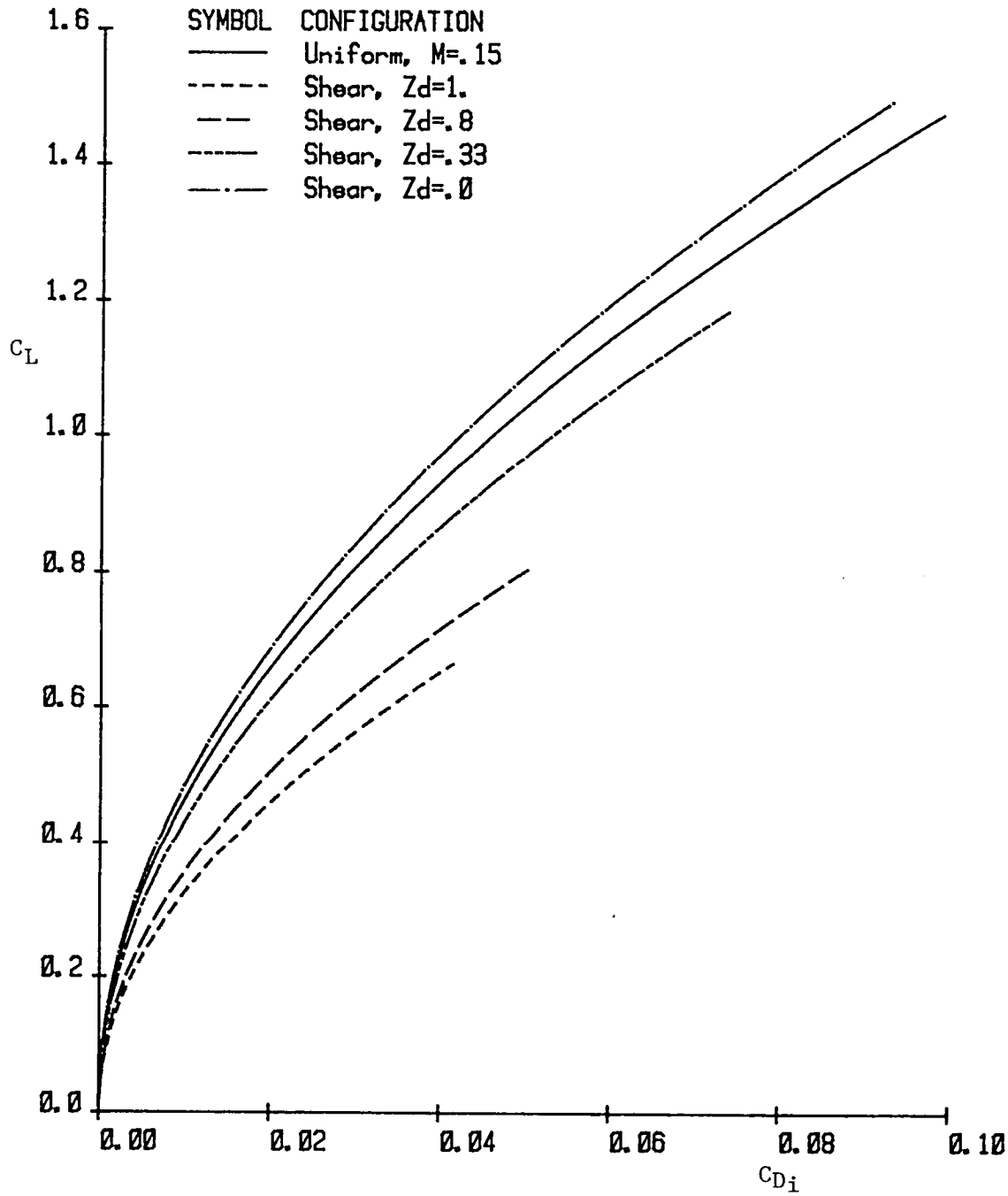

(b) C_L Versus C_{D_i}

Figure 18 Continued

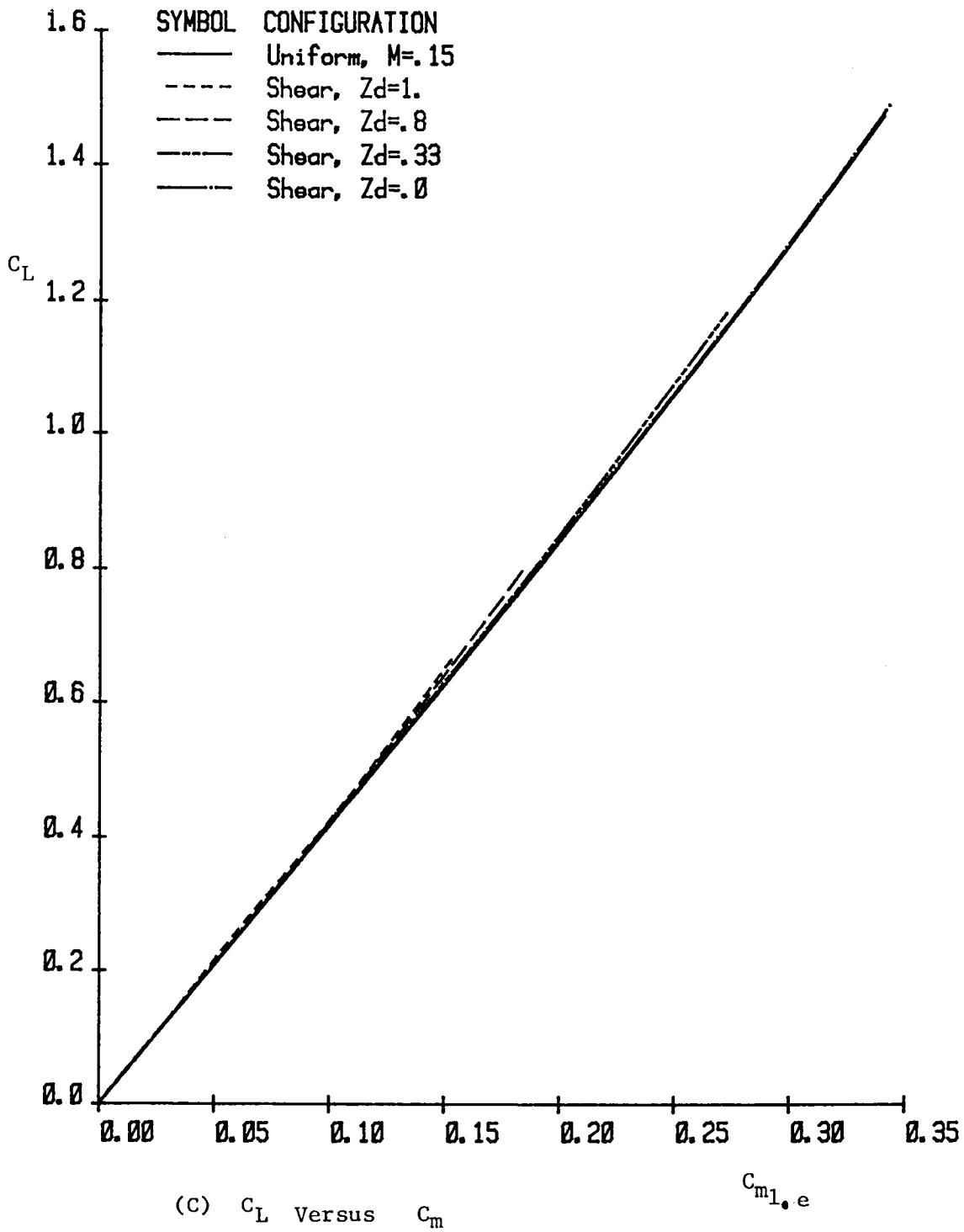

(C) C_L Versus C_m

Figure 18. Concluded

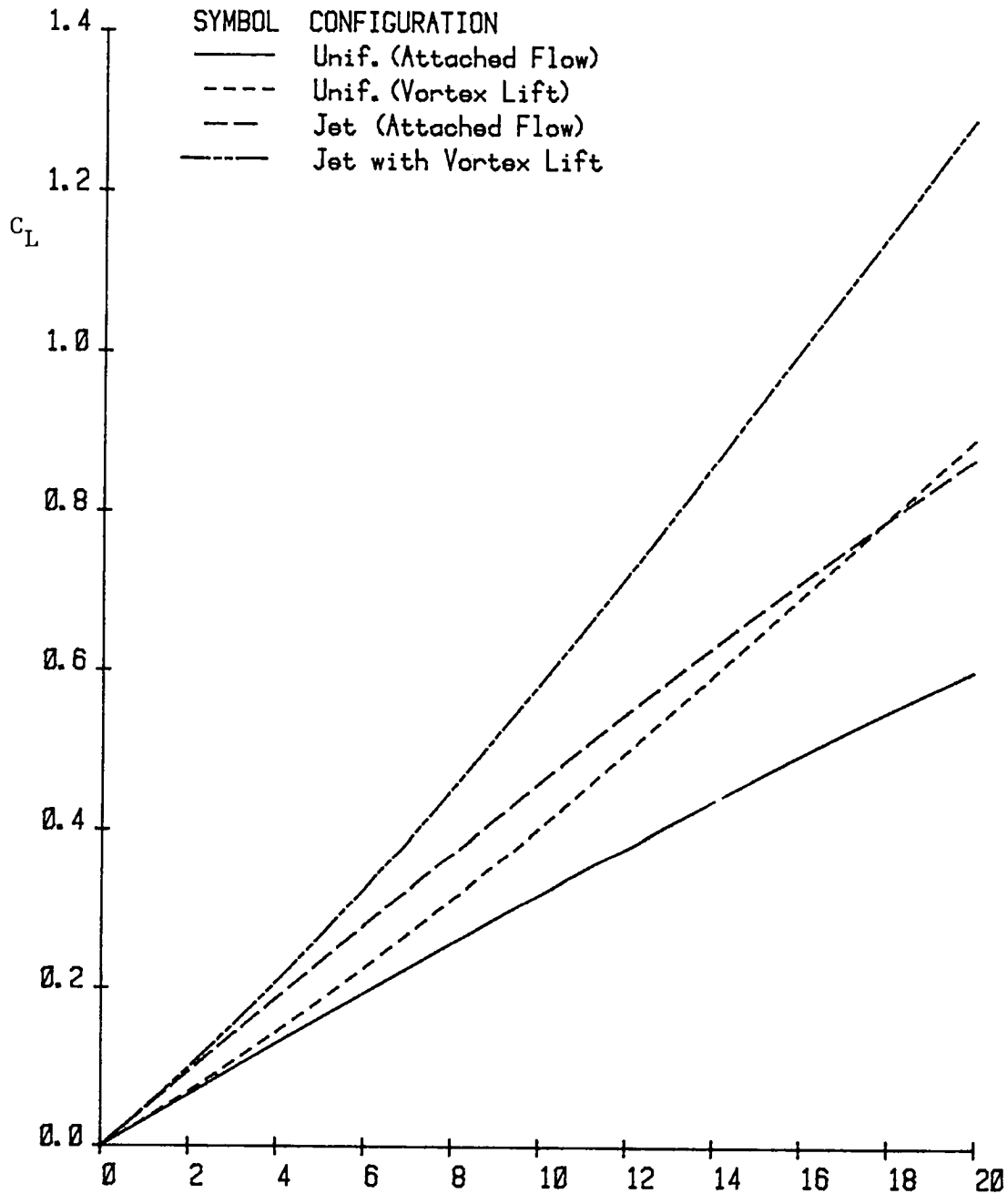

(a) C_L Versus α

Figure 19. Longitudinal Aerodynamic Characteristics of Flat Delta Wing ($\Lambda=70^{o}$) in Jet Flow. Reference Dynamic Pressure = 0.5 $\rho_1 V_1^2$

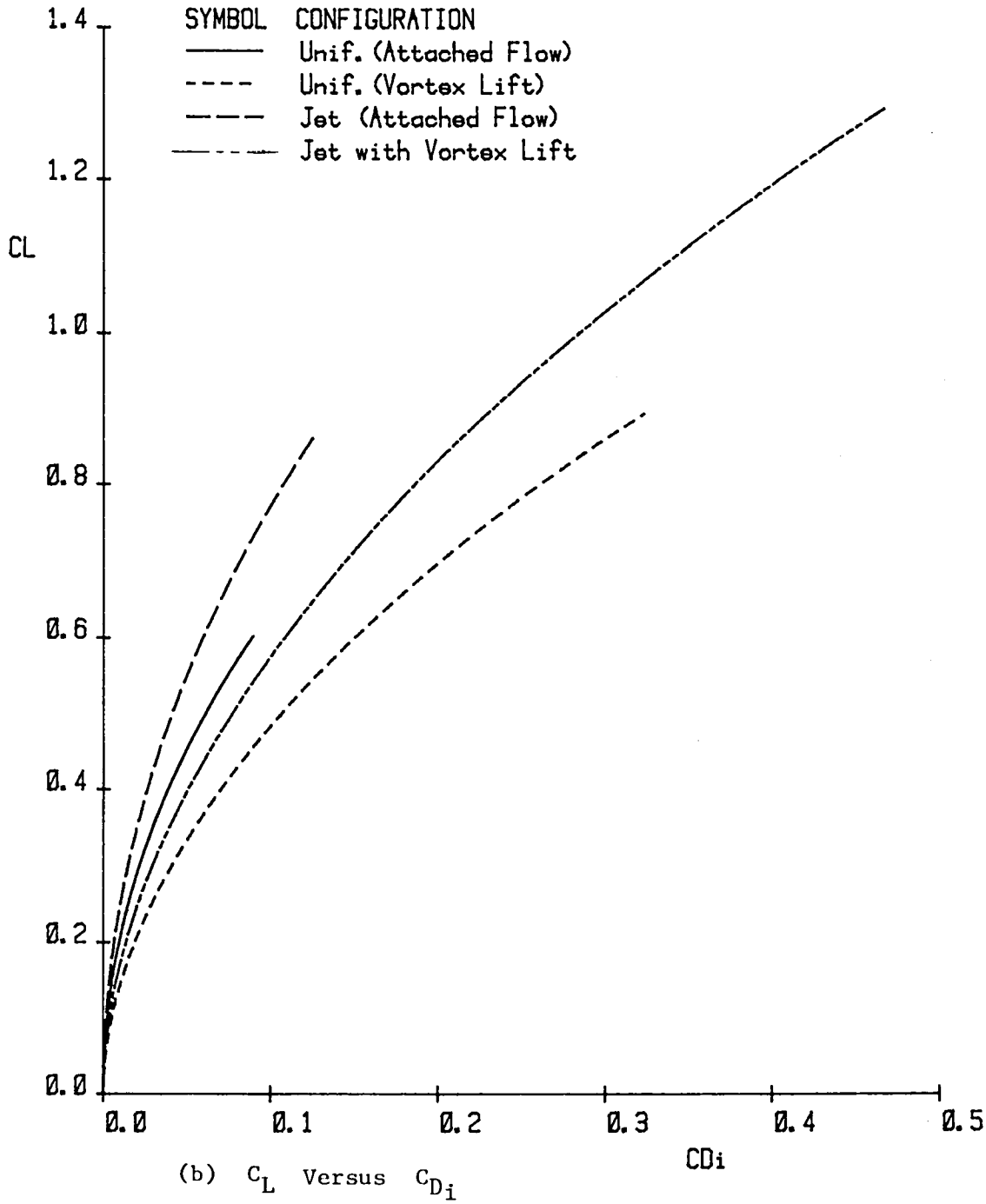

(b) C_L Versus C_{D_i}

Figure 19. Continued

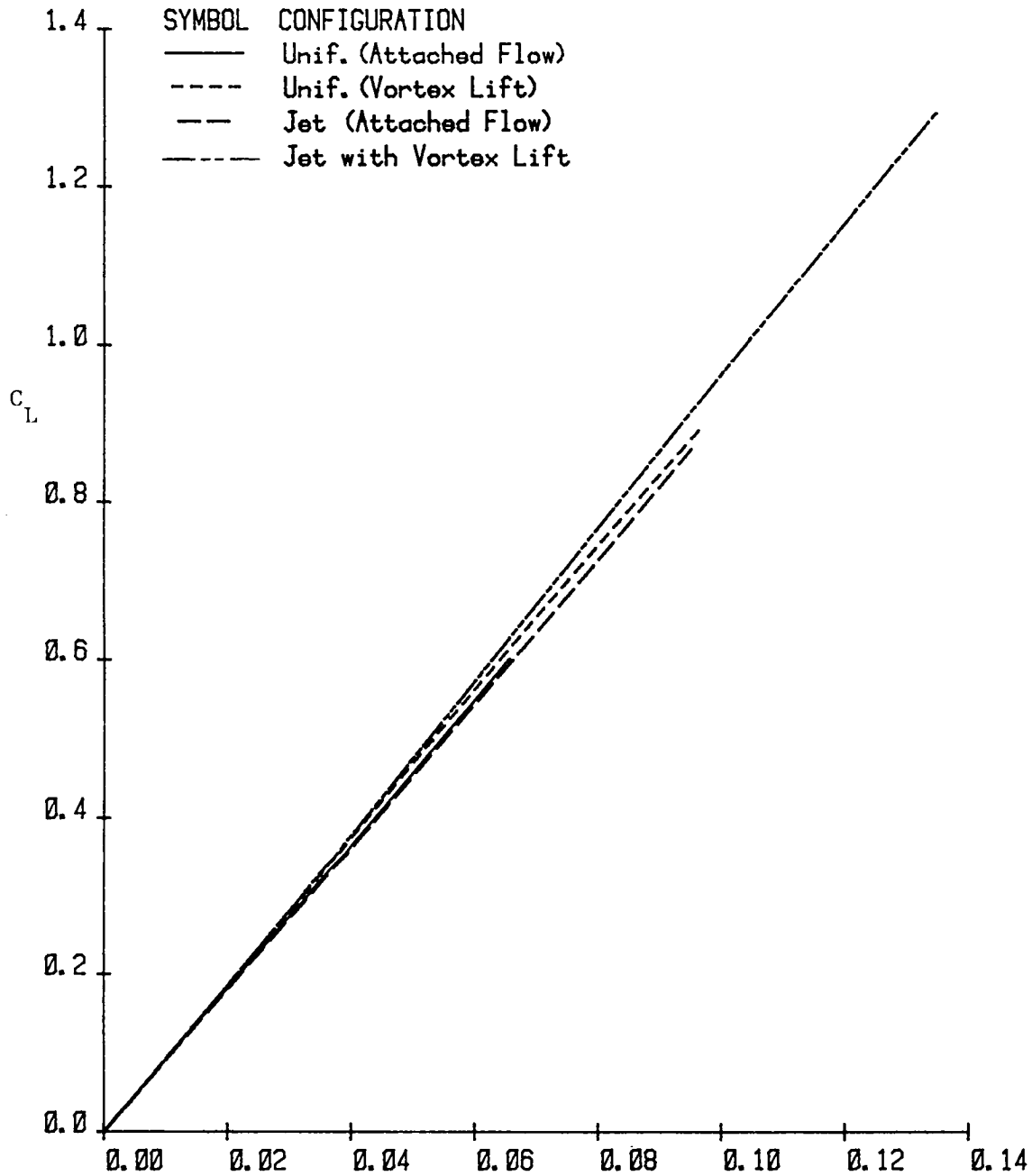

(C) C_L Versus C_m

Figure 19. Concluded

1. Report No.	2. Government Accession No.	3. Recipient's Catalog No.
NASA CR-172233		

4. Title and Subtitle	5. Report Date
A Lifting Surface Theory in Rotational Flow	October 1983
	6. Performing Organization Code
7. Author(s)	8. Performing Organization Report No.
Mawshyong Jack Shiau and C. Edward Lan	CRINC-FRL-467-2
	10. Work Unit No.
9. Performing Organization Name and Address	
The University of Kansas Center of Research, Inc. 2291 Irving Hill Drive - Campus West Lawrence, Kansas 66045	11. Contract or Grant No. NAG1-75
	13. Type of Report and Period Covered June 1981-Dec. 1982 Contractor Report
12. Sponsoring Agency Name and Address	
National Aeronautics and Space Administration Washington, DC 20546	14. Sponsoring Agency Code 505-31-23-07

15. Supplementary Notes

Langley Technical Monitor: Neal T. Frink
Topical Report

16. Abstract

The partial differential equation for small-disturbance steady rotational flow in three dimensions is solved through an integral equation approach. The solution is obtained by using the method of weighted residuals. Specific applications are directed to wings in nonuniform subsonic parallel streams with velocity varying in vertical and spanwise directions and to airfoils in nonuniform freestream.

Comparison with limited known results indicates that the present method is reasonably accurate. Numerical results for the lifting pressure of airfoil, lift, induced drag, and pitching moments of airfoil, lift, induced drag, and pitching moments of elliptic, rectangular, and delta wings in a jet, wake, or monotonic sheared stream are presented. It is shown that, in addition to the effect of local dynamic pressures, a positive velocity gradient tends to enhance the lift.

17. Key Words (Suggested by Author(s))	18. Distribution Statement
Rotational flow Lifting surface theory Subsonic flow Steady flow	Unclassified - Unlimited Subject Category 02

19. Security Classif. (of this report)	20. Security Classif. (of this page)	21. No. of Pages	22. Price
Unclassified	Unclassified	74	A04

For sale by the National Technical Information Service, Springfield, Virginia 22161